Robust Energy Calibration Technique for Photon Counting Spectral Detectors

Stefano Vespucci, Chan Soo Park, Raul Torrico, and Mini Das

***Abstract*— This paper describes the implementation of a novel and robust threshold energy calibration method for photon counting detectors using polychromatic X-ray tubes. Methods often used for such energy calibration may require re-orientation of the detector or introduce calibration errors that are flux and acquisition time-dependent. Our newly proposed "differential intensity ratios" (DIR) method offers a practical and robust alternative to existing methods. We demonstrate this robustness against photon flux used in calibration, spectral errors such as pulse pile-up as well as the detector's inherent spectral resolution limits. The demonstrated significant insensitivity of the proposed DIR signature to detector spectral distortions and energy resolution is a key finding. The proposed DIR calibration method is demonstrated using Medipix3RX detectors with a CdTe sensor under varying flux conditions. A per pixel calibration using the DIR method has also been implemented to demonstrate an improvement over the global energy resolution of the PCD.**

***Index Terms*— Energy calibration, photon counting detectors, x-ray detector, spectral resolution, x-ray fluorescence, Medipix.**

I. Introduction

SEMICONDUCTOR quantum detectors capable of resolving and processing single photons are emerging as powerful tool for many imaging applications. Recent versions of these single photon counting detectors (PCDs) are capable of energy discrimination and intercommunication between pixels to reduce spectral distortions [1], [2]. Besides spectral discrimination, PCDs allow image acquisition with zero dark noise resulting in an improved image quality with the potential for several low-dose medical and biological application [3]–[7]. These common imaging techniques include x-ray fluorescence (XRF) [8], K-edge absorption [9], computerized tomography (CT) [10]–[12], phase contrast [13], [14], ptychography [15] and material decomposition techniques [16]–[20].

PCDs are direct conversion detectors that use semiconductor sensors to convert x-rays to charge clouds. Electronic discriminators allow a comparison of signal generated by the incident photons with internal electronic threshold values. These values are commonly denoted as "thresholds" for the PCD. This mechanism allows filtering of photons that have energies lower than that corresponding to the electronic threshold chosen by the experimenter. Energy calibration is a process of accurately assigning the energy value corresponding to an electronic threshold corresponding to a particular digital-to-analog converter (DAC) value. This energy calibration of PCD thresholds is a required procedure before effectively using the spectral capabilities of these devices.

A global energy calibration, performed for all the pixels in the PCD, may be sufficient for many applications. It determines the average energy response of all the pixels in the PCD. The inter-pixel manufacturing variations in the detector electronics (like threshold and gain variations) lead to slight differences in energy calibration between pixels [1], [21] This results in a globally reduced energy resolution in the PCD. By evaluating the energy response of each pixel independently, a significant improvement in the energy resolution can be achieved.

Electronic settings such as pixel gain or current levels within the detector require separate optimization based on a particular application. One must also ensure robustness of spectral response due to temperature sensitivity or unforeseen effects of slow radiation damage to the electronics. Thus a routine PCD calibration to check for stable spectral response is desirable. Fast, simple and robust methods would be required for routine calibrations when these detectors are used in a clinical setting in the future. Most existing energy calibration techniques are influenced by the detector's intrinsic resolution, which decreases with increasing energy. In this paper, we present a robust energy calibration method that overcomes these limitations. Aspects such as robustness of calibration techniques to varying acquisition times and to flux changes are also addressed. While the methods discussed in this paper are relevant to any photon counting detector, we demonstrate the proposed methods using Medipix3RX detector with a CdTe sensor. We also demonstrate the utility of our proposed method for per pixel calibration with improved spectral data.

A. Medipix3RX Detector

The Medipix3RX detector [1], [21], [22] is a direct conversion semiconductor hybrid pixel detector developed by an international collaboration based in CERN, Geneva. It has

Manuscript received August 3, 2018; revised September 29, 2018; accepted October 7, 2018. This work was supported in part by the U.S. Department of Defense (DOD) Congressionally Directed Medical Research Program (CDMRP) Breakthrough Award under Award BC151607 and in part by the National Science Foundation CAREER Award under Award 1652892. *(Corresponding author: Mini Das.)*

The authors are with the Department of Physics, University of Houston, Houston, TX 77204 USA (e-mail: mdas@central.uh.edu).

Color versions of one or more of the figures in this paper are available online at http://ieeexplore.ieee.org.

Digital Object Identifier 10.1109/TMI.2018.2875932

spectroscopic capabilities allowing up to eight electronic thresholds to be used for energy discrimination.

Medipix3RX detector consists mainly of two parts: the sensor, where the incoming photons are converted into electron-hole pairs, and the Medipix3RX application specific integrated circuit (ASIC) electronics, where the signal is processed for readout. The sensor is usually a semiconducting material such as Si, CdTe or GaAs and consists of a diode structure. A grid of equally spaced metallic bump-bonds behind the sensor allows for virtual pixellation. Each bump-bond is connected to the ASIC electronics, allowing for independent readout for every pixel.

A reverse bias voltage is applied to the sensor in order to deplete the diodes junction interface region and to create an electric field within the sensor. This voltage depends on a number of factors such as sensor material, sensor thickness and doping concentration within the sensor. The electric field allows the generated charge cloud to drift toward the ASIC electronics, where the signal is processed. The incident x-ray photons generate charge cloud, which is then collected at the electrode and readout for each pixel. The external electric field helps to minimize the lateral diffusion of charge cloud, thereby reducing charge sharing effects. Critical spectral errors can result if the charge cloud is partially collected by the neighboring pixels and read erroneously as a low-energy photon [23], [24].

The Medipix3RX detector unit has an active area that is composed of 256 $\times$ 256 pixels, each measuring 55 $\mu m \times$ 55 μm. The various operating modes for Medipix3RX can be found in prior literature [1], [2], [23], [24]. The charge summing mode allows one to utilize the built-in correction for charge sharing via inter-pixel communication enabled in the hardware [1]. This is a desirable mode for most of our applications due to improved spectral fidelity. For Medipix3RX, one can further choose a fine-pitch mode that allows the highest spatial resolution of 55 μm which is also desirable for many of our applications. Hence the energy calibrations shown in this paper are done in a fine pitch mode with charge sharing correction.

For a selected DAC threshold value, the detector pixels count the number of photons having an energy above that of the energy E_i represented by the selected threshold. For any given threshold energy E_i, the integral mode count ($I^{int}(E_i)$) is:

$$I^{int}(E_i) = \int_{E_i}^{\infty} \Phi(E) D(E) dE, \qquad (1)$$

where $\Phi(E)$ is the spectrally dependent incident x-ray flux and $D(E)$ the detector response function, which takes into account factors such as absorption efficiency, flux dependence and spectral distortions like charge sharing and pile-up.

A common operation which is performed in order to monitor the spectral energy response of the detector as a function of the digital-to-analog-converter (DAC) threshold value is referred to as the threshold DAC scan. Here the photons collected for each DAC threshold is recorded (for a selected time interval) as the threshold value is systematically incremented at finite intervals. As seen in Eq. 1, this data represents the integral of counts above a given threshold as we vary the threshold level during the scan. This integral-mode spectra has to be differentiated to obtain the photon counts corresponding to each threshold (or the corresponding energy) referred to as differential mode spectra in this paper.

Accurate energy calibration (deciphering what the corresponding energy is for each threshold) requires known sources of x-ray emission or absorption to be used as sharp reference points. With at least three reliable measurements, a threshold-energy calibration curve can be obtained, which then allows one to match any arbitrary threshold to the corresponding x-ray energy. Some reference energy sources used are radioactive sources, x-ray fluorescence sources [25], peak x-ray source emission (referred to as kVp calibration) [26], [27] and K-edge of any given material. Some drawbacks of these methods are the following: low count rates when using radioactive source emissions as reference; the need for re-orienting the detector when using metal fluorescence lines for reference (as shown in Sec. II-B1); the flux-dependent drifting of calibration curve when using a kVp method (as shown in Sec. II-B3); the broadening of absorption edge due to limited detector spectral resolution when using K-edge absorption method (as shown in Sec. II-B2). In Sec. II-C we describe a robust calibration method against source flux and the limited detector inherent resolution. An x-ray fluorescence method (described in Sec II-B1) is used as a gold standard to compare our new approach. While XRF method requires re-organizing the imaging setup and time consuming, the results obtained are fairly robust due to the relatively low count rate. The presence of a sharp emission peak also offers accuracy in spite of the spectral broadening due to the detector resolution.

II. Experimental Methods

A. Medipix3RX Measurement Setting

All the experiments reported in this paper are performed by using a micro-focus x-ray tube L8121-03 from Hamamatsu with a Tungsten anode and with operating limits of up to 150 kV and 500 μA. The Medipix3RX detectors with 1000 μm thick CdTe sensor was used, with an applied bias voltage of $-$500V to the sensor. An equalization for threshold dispersion among pixels were performed prior to the measurements. This operation fine tunes the thresholds in each pixel within the matrix to enable improved inter pixel response uniformity.

For each detected photon, the pixel electronics require a finite time to collect and process the signal. The pixel remains in an inactive state for this interval of time (called the dead time, τ) leading to what is known as a dead-time loss [28]. Hence, quasi-coincident photons may be recorded as a single event for high flux-rates. The result is an apparent reduction in the photon counts and a distortion of the measured energy spectrum due to pulse pile-up [28]. The magnitude of spectral distortion due to pile-up is proportional to the incident flux rate [28].

The detector dead time was estimated by fitting the measured flux rates to an analytical paralyzable model [22], [24] (see Eq. 2) for a range of photon fluxes obtained by changing

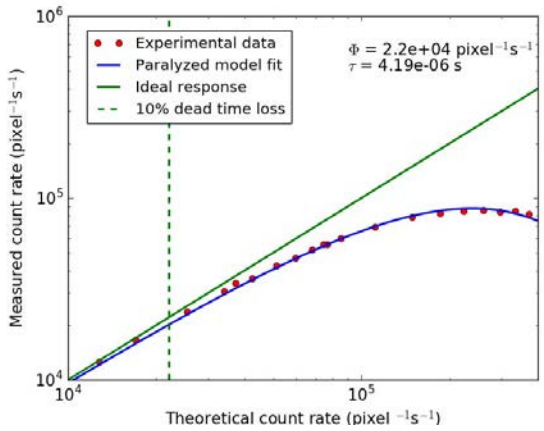

Fig. 1. Measured photon fluxes as function of the expected fluxes for a paralyzable model. The vertical dashed line shows the position of the 10% dead time loss for Medipix3RX CdTe detector.

the source detector distances.

$$\Phi_{meas} = \Phi_{est} e^{-\Phi_{est}\tau}, \tag{2}$$

where Φ_{meas} and Φ_{est} are the measured and estimated photon fluxes per pixel respectively, given in unit of s^{-1} and τ is the pixel dead time in seconds. Φ_{est} is extrapolated from experimental data measured at very low count rates when pile up effect is negligible.

Fitting the data acquired at increasing x-ray flux rates to this paralyzable model (Figure 1) yielded a dead time of 4.2 μs for the Medipix3RX detector with a 1000 μm thick sensor. This value is comparable with what is found in the literature [29] for similar detector settings. Flux rate levels used for the experiments in this paper range from $\approx$ 43 counts/s/pixel to $\approx 1.5 \times 10^5$ counts/s/pixel. Pile-up effects might be considered limited only for photon flux values below $\approx 2.5 \times 10^4$ counts/s/pixel, resulting in at least 10% dead time loss (shown by vertical dashed line in Fig. 1).

B. Existing Calibration Techniques

A number of existing energy calibration methods were tested and compared against our newly proposed method (Sec.II-C).

1) X-Ray Fluorescence: X-ray fluorescence (XRF) emission peaks from metals can be used as references for energy calibration of PCDs. Since XRF signal is low compared to the primary x-ray beam, for these measurements, the detector is positioned at 90° with respect to the target and the primary beam (Fig. 2(a)).

The x-ray source was operated at 250 μA and 100 kV. The threshold scans were performed for all targets by using an acquisition time of 1 s per frame, and varying the DAC threshold from 20 to 150, using a step size of one DAC threshold (corresponding to $\approx$ 1 keV). The values of $K_{\alpha 1}$, $K_{\alpha 2}$ and K-edge (corresponding to K shell electron binding energy) from the elements used for our XRF and K-edge calibration are listed in Table I. The resulting XRF calibration line is shown in Fig. 3.

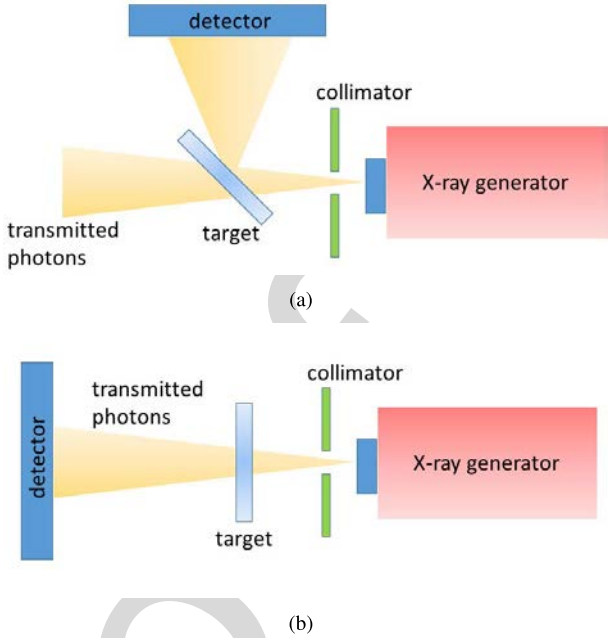

Fig. 2. Sketch showing the experimental set up used for (a) XRF and (b) K-edge absorption measurements.

TABLE I
LIST OF THE ELEMENTS USED FOR XRF CALIBRATION AND CORRESPONDING $K_{\alpha 1}$, $K_{\alpha 2}$ AND K-EDGE EMISSION VALUES [30]

Element	$K_{\alpha 1}$ (keV)	$K_{\alpha 2}$ (keV)	K-edge (keV)
Zr	15.77	15.69	18.00
Sn	25.27	25.04	29.21
Nd	37.36	36.85	43.57
Gd	43.00	42.31	50.21
W	59.32	57.98	69.52
Pb	75.00	72.80	88.01

Energy resolution (ΔE) can be indicated in terms of the full width at half maximum (FWHM). By using K_α emission peaks from target materials ΔE, and the relative energy resolution ($\frac{\Delta E}{E}$), was measured at energies corresponding the XRF K_α from Zr, Gd, W and Pb (showing well defined Gaussian peaks). These are shown in Fig. 3 (b - c) respectively.

Due to the need for re-arranging the detector, XRF calibrations may not be accessible in a PCD CT system. However energy calibrations using XRF is very precise and reliable. For this reason, we use the energy calibration from XRF as reference for all the other calibration methods. In the remaining sections of this paper, all the threshold values are expressed in energy units based on the corresponding XRF calibration.

2) K-Edge Absorption: Threshold calibration using K-edge absorption uses a simple transmission geometry (Fig. 2(b)). The energy dependent attenuation coefficients of target material are measured and the K-absorption edge is used as reference in the calibration. The linear absorption coefficient measured from a W plate (0.1 mm thick) as a function of varying energy is shown in Fig. 4. This data was acquired by scanning the energy threshold from $\approx$ 20 keV to $\approx$ 120 keV,

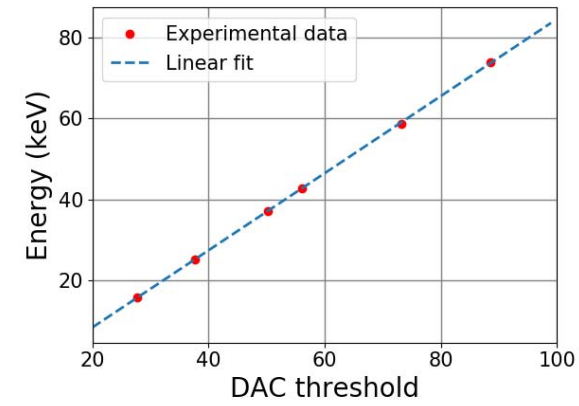

(a)

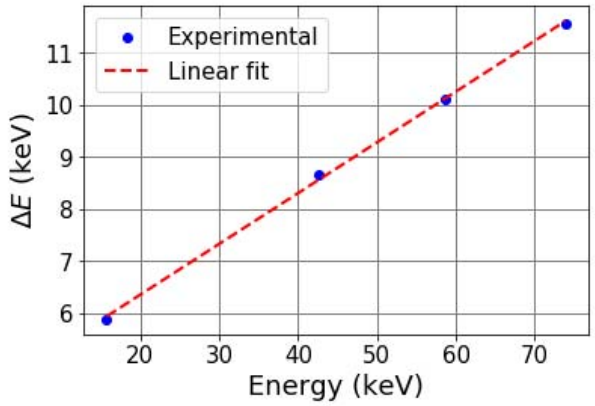

(b)

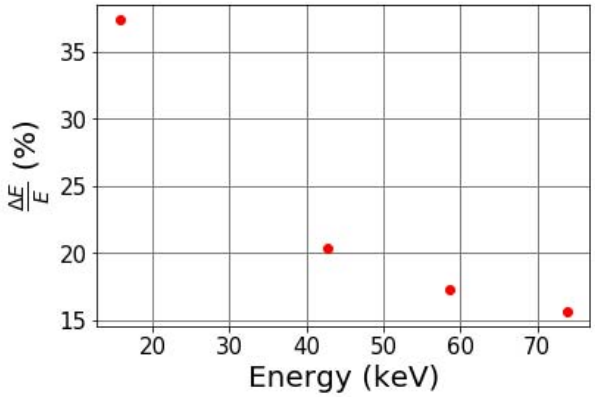

(c)

Fig. 3. (a) Threshold energy calibration obtained for the Medipix3RX chip having a CdTe 1000 μm thick sensor, using K_α XRF emissions from the elements listed in Table I. (b) Energy resolution (FWHM) and (c) relative energy resolution ($\frac{\Delta E}{E}$) measured from Zr, Gd, W and Pb targets.

using a threshold step equivalent of $\approx$ 1 keV. The energy values shown on x-axis correspond to the respective thresholds (based on XRF calibrations in Sec. II-B1). For reference, the K-edge energy (69.52 keV) of the W target is shown with a vertical dashed line (obtained from the NIST database [30]). As observed, due to the limited energy resolution of the detector as well as the non-ideal and flux dependent detector spectral response, the measured transitions at the characteristic

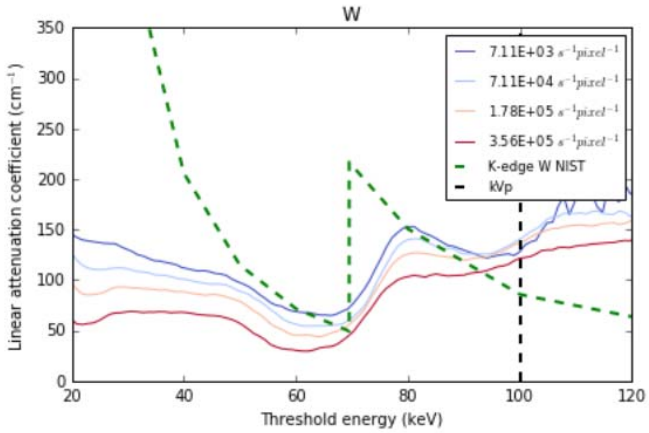

Fig. 4. Linear attenuation coefficient measured from a W target.

K-edge energies are quite broad. Hence it is difficult to precisely determine the DAC threshold value corresponding to the K-edge energy, making it a challenge to use this method for energy calibration [31]. Fig. 4 also shows the strong spectral distortion introduced by the detector for energies well below the K-edge as well as near the kVp.

A strategy to mitigate these issues due to the limited detector energy resolution is described in Sec. II-C.

3) X-Ray Tube Voltage Peak: Peak voltages (kVp) corresponding to the x-ray tube spectra has shown to be useful references for energy calibration of PCDs [26], [27], [32]. These reference points correspond to the maximum energy for photons emitted from a polychromatic x-ray tube for a set acceleration voltage [26], [27], [32]. One advantage of this method is the continuous range of energies available from the x-ray tube and the simple setup requiring no additional hardware or target materials.

The method is based on the determination of the highest energy (and corresponding threshold) at which all the pixels in the detector detect zero photons, which should occur at the tube kVp. However, since the energy response of pixels in the matrix have a normal distribution, such a sharp cut off is not seen. During a threshold scan about 50% of the total pixels in the detector would count at least one photon at the DAC threshold corresponding to the peak energy of the x-ray spectrum [26]. This threshold value for which 50% of pixels are ON can be treated as the reference for the peak tube voltage (kVp) [26], [27].

By repeating this procedure for a number of kVp values for which the x-ray tube can be turned on sequentially, a calibration line can be obtained [26], [27]. Although the kVp method provides quick results, a number of non-converging behaviors have been reported [27], [32] and observed by the authors in our own laboratory. The calibration curve shifts with varying exposure times and changing flux. This effect has been explained in terms of stochastic noise building up over the time. Sources of noise can be for example thermal noise or pile-up effects [32].

We tested this divergence from ideal behavior for various flux conditions obtained by changing tube currents to 50 μA, 100 μA, 150 μA, 250 μA and 350 μA for a set source to

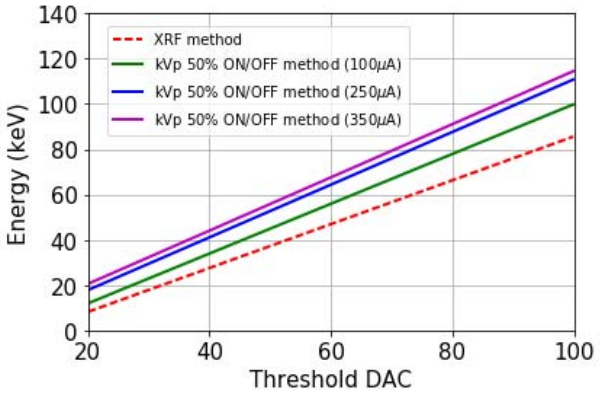

Fig. 5. Comparison between calibration lines obtained by applying the kVp method on dataset obtained using three x-ray tube currents (100, 250 and 350 μA) and the standard XRF method.

detector distance of 46 cm. For each current value, a range of x-ray source peak voltages were used, from 25 kVp to 125 kVp with a step of 25 kV to get a calibration line corresponding to each flux rate determined by the tube current (see Fig. 5).

Figure 5 shows three calibration lines, obtained by applying the kVp method to three flux levels by operating at x-ray tube currents, 100 μA, 250 μA and 350 μA respectively. The XRF based calibration is shown for comparison as well. Strong dependence of calibration on photon flux is evident. A deviation of up to 30 keV can be observed for even a photon flux that is well below the 10% dead time loss flux rate. The flux levels in clinical CT systems are much higher than what is used in our benchtop system and much larger deviations and uncertainty in calibrations could be expected. The newly proposed calibration method in this paper (Sec. II-C) are aimed for improved robustness against photon flux used during calibration in kVp method. The following sections describe the DIR method as applied to both kVp and K-edge type calibration methods for a PCD.

C. Differential Intensity Ratios Method

The method is based on our observation that the differential or relative variations in photon counts is significantly sharper than the actual variation of counts at the K-absorption edge as well as at the peak energy of the x-ray spectrum (kVp). The method is summarized below for a general case when a K-edge material is used for reference with specific examples presented in subsequent sections. First, the energy dependent integral mode photon counts at the detector is measured with and without the target material placed between the x-ray tube and the detector (setup shown in Fig. 2(b)). For each threshold ($i = 1, 2, \ldots$), a spectrally varying intensity I^{int} and I_0^{int} is obtained with and without the target. The intensity data acquired in integral mode using the Medipix3RX can be described as:

$$I^{int}(E_i) = \int_{E_i}^{\infty} \Phi(E) e^{-\mu(E)x} D(E) dE \tag{3}$$

$$I_0^{int}(E_i) = \int_{E_i}^{\infty} \Phi(E) D(E) dE, \tag{4}$$

where $\Phi(E)$ is the incident x-ray spectrum, $\mu(E)$ and x are the linear attenuation coefficient and thickness of the target and $D(E)$ is the detector response function which includes flux dependence. I^{int} and I_0^{int} represent the target data and the flat field data respectively.

The energy spectrum is obtained by differentiating the integral data with respect to the discrete threshold values:

$$I_i = \frac{I_i^{int} - I_{i+\Delta i}^{int}}{\Delta i} \tag{5}$$

$$= \int_{E_i}^{E_{i+\Delta i}} \Phi(E) e^{-\mu(E)x} D(E) dE \tag{6}$$

$$I_{0,i} = \frac{I_{0,i}^{int} - I_{0,i+\Delta i}^{int}}{\Delta i} \tag{7}$$

$$= \int_{E_i}^{E_{i+\Delta i}} \Phi(E) D(E) dE \tag{8}$$

A flat field correction, e.g. the division between data acquired with the target and the data acquired without the target,

$$\frac{I_i}{I_{0,i}} = \frac{\int_{E_i}^{E_{i+\Delta i}} \Phi(E) e^{-\mu(E)x} D(E) dE}{\int_{E_i}^{E_{i+\Delta i}} \Phi(E) D(E) dE} \tag{9}$$

$$\simeq \left\langle e^{-\mu(E)x} \right\rangle_i, \tag{10}$$

is performed for each threshold. If the flux difference with and without the target is very large leading to change in detector response functions, the D(E) values in the numerator and denominator of Eq. 9 would only approximately be the same. This approximation is noted in Eq. 10. Finally, the flat field corrected intensities can be differentiated with respect to the applied threshold,

$$DIR = -\frac{\partial}{\partial i} \frac{I_i}{I_{0,i}}. \tag{11}$$

The trend of DIR would reveal Gaussian-like peaks at K-edge energies for the target material and at the kVp of x-ray tube spectrum. These observed peaks can be used as references to find energies corresponding to the electronic thresholds. By using multiple K-edge materials in the beam path simultaneously, one can acquire a calibration line in a single shot. The K-edge from high energy efficient sensor material (e.g. Cd and Te) can also be often used as a reference point.

The newly proposed calibration method was applied to the experimental dataset acquired from K-edge experiments described previously in section II-B2.

Figure 6(a) shows threshold scans acquired in integral mode by monitoring the photons transmitted through a Gd target, see Eq. 3. In order to compare threshold scans acquired under different photon flux conditions, counts displayed in the figure were normalized by the total number of photon counts for the entire scan.

Figure 6(b) shows the corresponding differential mode data with flat field correction. This data corresponding to $\frac{I_i}{I_{0,i}}$ (see Eq. 9) shows three distinct transitions. Two of these peaks are at K-edge energies corresponding to Cd (26.7 keV, from the CdTe sensor) and to Gd target (50 keV). The third peak is from the peak energy (100 keV) corresponding to the

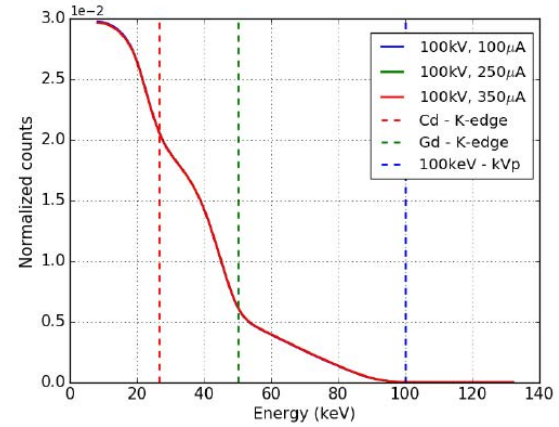

(a)

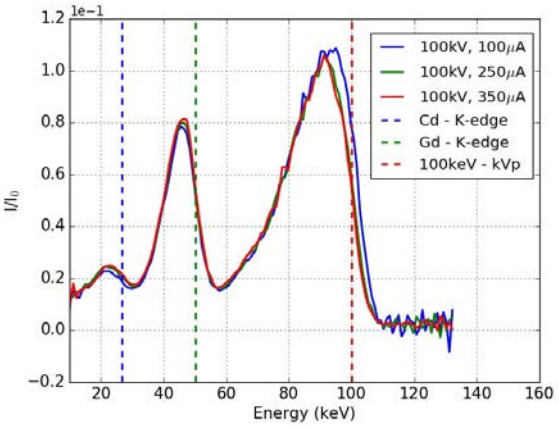

(b)

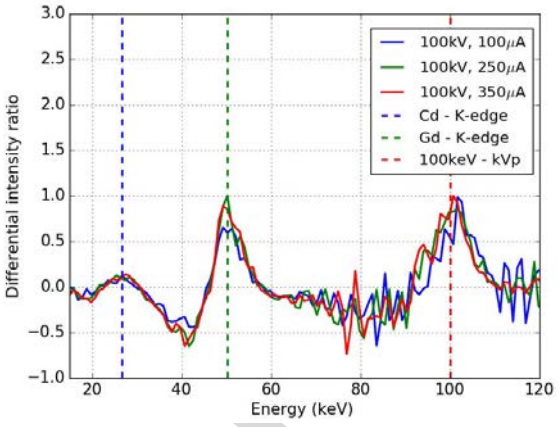

(c)

Fig. 6. Results from the new implemented method from Gd. (a) Threshold scans (see Eq. 3); (b) division between I and I_0 (see Eq. 9) (c) differential intensity ration (see Eq. 11).

x-ray spectrum. These reference energies are highlighted by vertical dashed lines in red, green and blue respectively in Fig. 6(a-c). Figure 6(c) shows the DIR plot (see Eq. 11) following the differentiation operation applied to the data shown in Fig. 6(b). The noise seen in this data is a result of differentiation. A smoothing operation can resolve this noise effectively (shown later in Fig. 8).

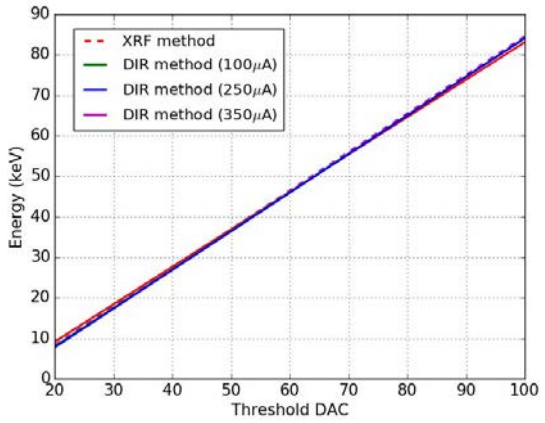

Fig. 7. Comparison between calibration lines obtained by applying DIR and XRF methods.

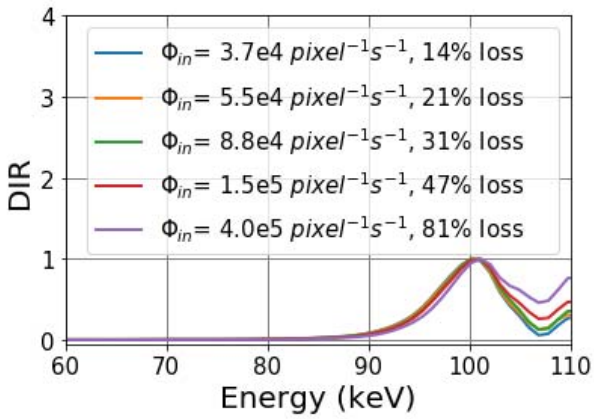

Fig. 8. Peaks obtained by applying the proposed method to dataset obtained using a x-ray tube peak voltage of 100kVp and different photon fluxes.

The peaks are clearly visible at all the three characteristic energies in Fig. 6(c). The DAC threshold corresponding to the characteristic energies is obtained via a Gaussian fit. In order to have additional data points, the procedure was also repeated for the W target (K-edge at 70 keV) in the beam path, and a calibration line was obtained. The position of the peaks in Fig. 6(c) appear to be negligibly dependent on the x-ray tube current value, at least for the range of currents used in our experiments. A comparison between the XRF and DIR calibration lines obtained using different x-ray tube current values is shown in Fig. 7. Please note that the energy resolution of PCD is not improved by applying the DIR method. The advantage, compared to conventional absorption measurements is that the DIR approach localizes the point where the K-edge transition occurs thus allowing a more accurate and robust energy calibration for the detector. Spectral inaccuracies due to calibration can add to the effects of distortions when collecting spectral data using PCDs.

Although the DIR peak seen at the characteristic K-edge energies are clearly related to a property of the target material,

i.e. the DIR peak is the result of the sudden change in the signal occurring at the K-edge, the peak found at the kVp energy is not. It is possible, indeed, to reveal a kVp DIR peak by applying the DIR method to any two dataset acquired under different photon fluxes and with no target material in the beam path. This is described more in detail in the next section. This observation suggests that the origin of the kVp peak has to be attributed to the detector response, D(E), which is flux dependent [28].

D. Robustness of the DIR Method Against Photon Flux

In order to examine the use of DIR method solely to kVp references, we applied the proposed procedure only to the flat field threshold scans (no target in the beam path) obtained at two different tube currents. In this case Eq. 11 can be re-written as:

$$DIR = -\frac{\partial}{\partial i}\frac{I_{0,i}^{ref}}{I_{0,i}^{n}}, \tag{12}$$

where $I_{0,i}^{ref}$ and $I_{0,i}^{n}$ are any two dataset acquired with the same experimental conditions but different x-ray tube currents. Furthermore, in order to demonstrate the robustness of the method against the photon flux, a range of photon fluxes were used, this time well above the 10% dead time loss. Flux rates of 1.9×10^3, 3.7×10^4, 5.5×10^4, 8.8×10^4, 1.5×10^5 and 4.0×10^5 counts pixel^{-1}s^{-1}, corresponding to dead time losses of 0.8%, 14%, 21%, 31%, 47% and 81% were used.

In our case, $I_{0,i}^{ref}$ consisted of the dataset acquired under the lowest flux (1.9×10^3 counts pixel^{-1}s^{-1}). $I_{0,i}^{n}$ consisted of the datasets acquired using other larger flux rates. In order to eliminate high frequency differentiation noise (see Fig. 6), data were first smoothed by using a Savitzky-Golay filter, showing peak shape preservation properties [33].

The result of this experiment (shown in Fig. 8) confirms that the peak positions from DIR do not change significantly with the incident photon flux, demonstrating the excellent stability of this method against variations in the photon flux.

A possible explanation for the origin of the kVp DIR peak is the following. While the true photon counts would diminish to zero above the x-ray kVp (see Fig. 6(a)), the peak shown in the DIR is only the result of differential distortions in the spectrum due to variations in PCD response to flux. This can be possibly attributed to effects such as pulse pile up that are not immediately visible from spectral measurements at low fluxes (such as in Fig. 6(a) and Fig. 9(a) below. Figure 9(a) shows two normalized flat field energy spectra, acquired with photon fluxes below 10% dead time losses, where pile up effects are limited. Ideally, normalized datasets not affected by pile up spectral distortion should appear identical. At first glance, indeed, energy spectrums shown in Fig. 9(a) appear very similar to each other. However, upon closer look, Fig. 9(a) (see inset showing the zoom-in plot for energy around 100 keV) shows higher counts above the kVp (indicated by the vertical black dashed line) for the dataset acquired with higher flux. Such a difference between spectrums is enhanced by the division step of the DIR method, as shown in Fig. 9(b). There is an energy range where the two spectrums are not significantly different (i.e. their ratio is close to unity, as indicated by the horizontal red dashed line). At energy range around the kVp, instead, the division shows a peculiar s-shaped transition, indicating a sudden change in the

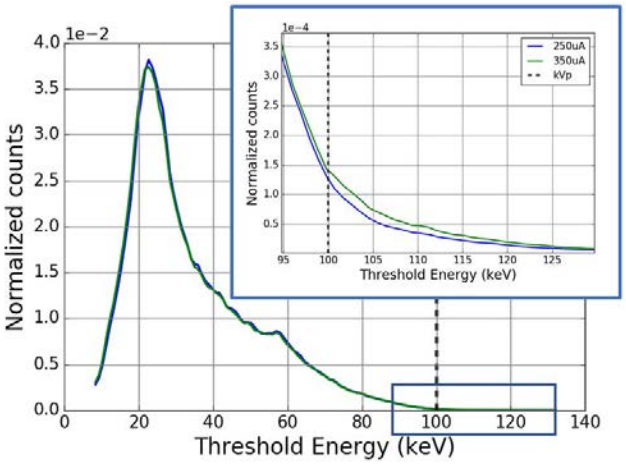

(a)

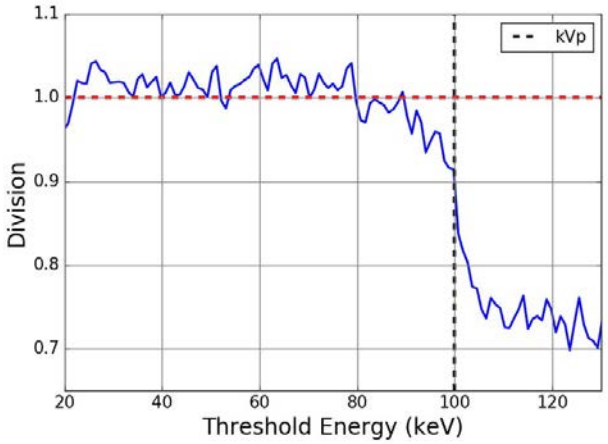

(b)

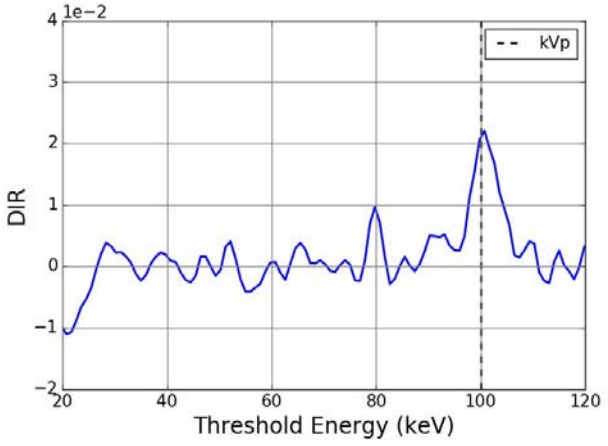

(c)

Fig. 9. DIR method applied to low flux flat field images. (a) Normalized energy spectrums highlighting dataset differences at the kVp energy; (b) ratio between datasets and (c) DIR peak at the kVp.

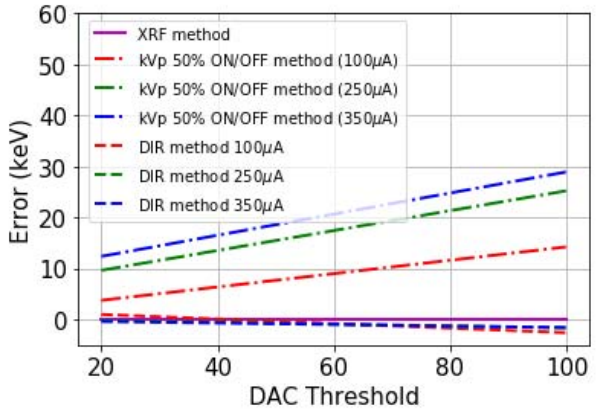

Fig. 10. Comparison between calibration methods. Discrepancy between DIR and kVp calibration methods and the XRF.

TABLE II
COMPARISON BETWEEN THE DEVIATION OF THE PRESENTED METHODS FROM THE XRF CALIBRATION LINE

RMS deviation from the XRF calibration (keV)		
	kVp method	DIR
100 μA	9.45	1.31
250 μA	17.99	0.99
350 μA	21.19	1.05

spectral distribution for this ratio at the kVp energy. The DIR peak seen at the kVp, shown in Fig. 9(c), directly reflects such a sudden transition. Thus while changes due to pile up effect are not visible for most of the spectra, it becomes relevant in the spectral ratio obtained in DIR (and hence the spectral change with changing flux). This can be clearly seen at and immediately after the kVp energy as the only photons detected after that energy is due to pile up effect.

E. Comparison of Calibration Methods

A comparison of global calibration lines obtained with the previously presented methods is shown in Fig. 10. The deviations from XRF based calibrations against the original kVp method [26], [27], [32] and DIR calibration method under various flux conditions is represented as errors (in keV).

As seen in Fig. 10, throughout the full range of thresholds and fluxes used in our studies, the calibration lines obtained using the DIR method remains very stable. However, the calibration lines obtained using the 50% ON-OFF kVp method leads to significant divergence when a high flux is used. In the worse case it is of the order of 30 keV. A summary is shown in Table II, where the root mean square (RMS) deviation from the XRF calibration, for the different methods is shown. As seen, the maximum divergence (less than 3 keV) due to changing flux in DIR is well within the detector's inherent resolution.

We can deduce that the conventional kVp method is only applicable when a relatively low x-ray tube current is used, and the range of applicability should be evaluated beforehand, for example using the method suggested by Lee *et al.* [32]. Working at very low flux levels can lead to very long durations for the calibration. The safe choice of highest flux is difficult to decide *a priori* as this may vary with sensor type, thickness and other factors. The kVp method is also more sensitive to random stochastic variations in the detector count and to pile-up effects. Our proposed DIR method shows stability and accuracy with respect to change in the incident photon flux, when compared to the conventional kVp method. It appears to be unaffected by the flux ranges used in our experiments.

F. Per Pixel Calibration and Correction Method

In the studies described above (Sec. II-C and II-D), the DIR method was applied to a global threshold calibration. An improvement in the overall energy resolution of the detector can be obtained by applying the same method to each pixel independently. This would significantly minimize the effect of pixel to pixel variations (pixel gain variations and residual threshold variations). For measurements using Medipix3RX, the DAC TH is a unique global variable which can be controlled by the user and this value represents the global threshold for all the pixels. For a chosen global DAC TH, the corresponding energy is obtained by using the global calibration line, which is of the form:

$$\overline{E} = m_{glob} \times TH + c_{glob}, \tag{13}$$

where m_{glob} and c_{glob} are slope and intercept of the global calibration line respectively. Equation 13 represents the average energy calibration line for all the pixels in the detector when the global DAC TH is varied.

Although the threshold equalization procedure (see Sec. II-A) minimizes the pixel to pixel variations by introducing a threshold offset in each pixel, it does not correct for the gain variations existing between pixels. Effectively, this means that for a chosen global threshold TH during any measurement, the true energy calibration line equation is slightly different for each pixel in the detector and can be given by

$$E_p = m_p \times TH + c_p, \quad p = 1, 2, 3, \ldots, N \tag{14}$$

where m_p and c_p are the slope and the intercept of the calibration line for each pixel p respectively.

In order to obtain the true calibration line for each pixel in the detector, one can simply apply the DIR method (described in II-C) to each pixel independently after masking off any bad pixels. From variation in slope of these individual calibration lines, the pixel gain (keV/threshold DAC) variations across the matrix can be estimated. The spatial distribution of pixel gain within the chip and the corresponding histogram for our detector is shown in Fig. 11(a-b) respectively. The gain variations across the pixel matrix, expressed as the standard deviation of the slopes of the calibration lines, results to be of the order of 0.05 keV/threshold DAC. The coefficient of variation $\frac{\sigma}{\mu}(\%)$, is equal to 5.4%. Here μ and σ are the mean value and the standard deviation of the pixel gains across the pixel matrix.

Once the energy response of each individual pixel is determined, correction schemes can be applied for any particular measurement. One possible implementation is described below.

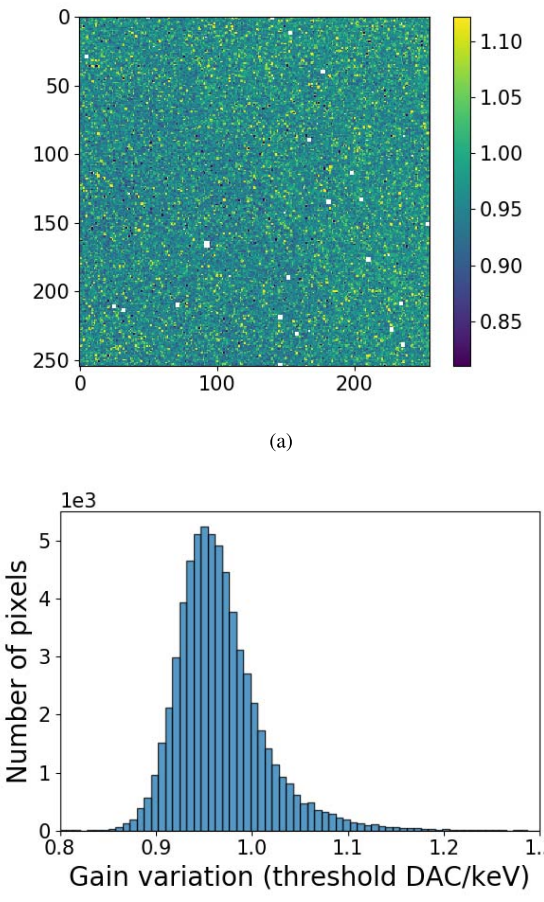

Fig. 11. Pixel gain variation across the PCD. (a) Spatial distribution of the gain and (b) corresponding histogram.

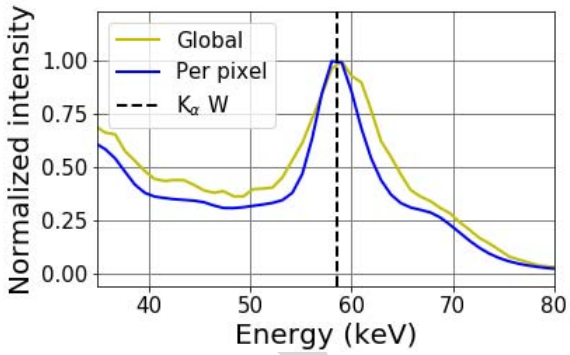

Fig. 12. Comparison between global and per pixel energy calibration. Correction procedure has been demonstrated using the K_α XRF peak recorded from a W target.

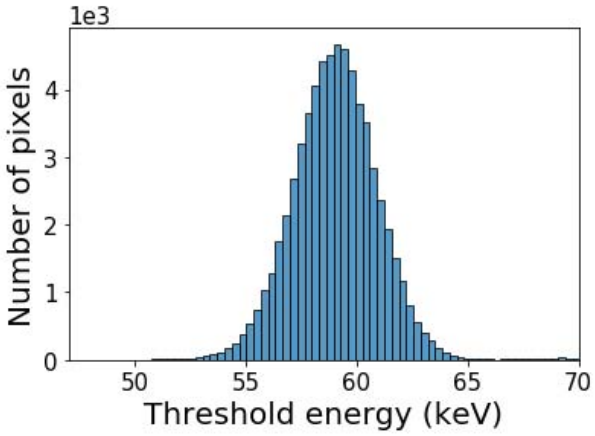

Fig. 13. Threshold dispersion measured at 58.65 keV.

The inter pixel variations can result in deviations in slopes of their individual calibration lines. Thus for any given measurement with a user specified DAC TH, the corresponding calibration energy E_p (See Eq. 14) of pixels may vary significantly from the global $\overline{E}$ (See Eq. 13), effectively reducing the detector's energy resolution. For uniform illumination across the detector and for a chosen DAC TH, this results in each pixel collecting x-rays above slightly different energies (E_p) instead of $\overline{E}$ (with a deviation $\Delta E_p = \overline{E} - E_p$), resulting in varying counts per pixel (I_p) (see Eq. 6) across the detector. Reducing the effect of gain variations and the resulting in-homogeneity in energy calibration across pixels amounts to effectively accounting for and correcting these deviations in counts. The deviation in counts (ΔI_p) for a chosen DAC TH, can be estimated as $\Delta I_p = \frac{dI_p}{dE_p}\Delta E_p$ where $\frac{dI_p}{dE_p}$ can be obtained by interpolating I_p. A map of ΔE_p across the detector pixels can be obtained following a per-pixel calibration using DIR technique as described earlier. The corrected intensity for each pixel, I_p^{corr} can now be estimated as $I_p^{corr} = I_p + \Delta I_p$; completing the corrections for per-pixel energy calibration across the detector unit.

Such pixel by pixel correction procedure following an initial global DIR based calibration method is demonstrated here with the measured K_α fluorescence line of a W target. A comparison between the measured energy spectrum before and after the per pixel spectral correction is shown in Fig. 12.

For both calibration methods the figure shows the total counts (obtained by summing up photon counts of all pixels in the chip) as a function of the threshold energy, over a range of DAC thresholds corresponding to energies between 35 and 80 keV. For the per pixel calibration, the counts in each pixel were corrected as described above to account for inter-pixel variation in true energy threshold levels.

By using the global DIR calibration, a FWHM of ≈10 keV at 58.65 keV (the K_α emission line of the W) was measured, corresponding to an energy resolution of 17%. By using the pixel by pixel correction method, a FWHM of ≈7 keV, corresponding to an energy resolution of 12% was measured for the same energy. This shows how a pixel by pixel calibration significantly improves the overall PCD's energy resolution. This would be particularly useful for ASICs where interpixel gain variations are large and often much higher than what is found in Medipix detectors.

By monitoring the position of tungsten K_α emission line for each independently calibrated pixel, the DAC threshold variations between pixels can be estimated. By calculating standard deviation of the threshold energy positions among the pixels for the particular emission energy in the tungsten fluorescence, one can quantify the threshold dispersion. The measured threshold dispersion at 58.65 keV was found to be of the order of 4.48 keV, with a coefficient of threshold dispersion variation of ≈7.6% (see Fig. 13).

It is worth noting that the overall improvement in the PCD energy resolution only arises from inter pixel gain and residual threshold dispersion corrections. In principle, any robust and accurate calibration method (not necessarily the proposed DIR method) applied on a pixel to pixel basis followed by a correction in counts for each pixel to account for the variability would provide the same improvement in the overall energy resolution.

III. Conclusion

An overview of three methods used for calibrating the DAC threshold value of photon counting detectors has been presented, highlighting the strengths and the weaknesses of each method.

The XRF provides a precise method for PCD energy calibration. Its main limitation is the requirement for rearranging the experimental set up necessary for calibration. This is not always feasible in clinical imaging systems. We showed that the K-edge calibration method is limited by the detector's inherent energy resolution and by the significant detector's spectral distortion.

The conventional kVp calibration method proposed previously [26], [27] is the most practical in terms of continuously available reference energies from the x-ray tube. This method can be implemented without any additional components or targets for the calibration procedure and does not require realigning the detector as in XRF methods. However, this method does not yield robust calibration under varying flux or scan times.

In order to overcome these limitations, we propose a novel and simple alternative: a differential intensity ratios method which exploits the sharp spectral variation in the relative intensities at K-edges as well as at the kVp. The demonstrated significant insensitivity of DIR signature to detector spectral distortions and energy resolution is a key finding. The implementation of our novel approach was demonstrated for K-edge and kVp based energy calibration, offering stable and accurate results when compared to the XRF method. When applied as an alternative to conventional K-edge calibration, the DIR method allows precise localization of the K-edge transitions. This is otherwise difficult to determine because of the broadening introduced by the detector's energy resolution and spectral distortions. When used as a kVp method, the DIR offers significant stability against incident photon fluxes. The main advantage of DIR over XRF method is that no rearrangement of the source and detector positions is required. A convenient way to implement the proposed DIR method would consist of using two or more targets with K-edges simultaneously in the beam path while also exploiting the source kVp. Alternatively, one could simply apply the DIR method to multiple exposures with changing kVp values without the need for any target material in the beam path.

Finally, we demonstrated the advantages of a pixel by pixel calibration using the DIR method in improving the detector's spectral resolution. This is achieved by correcting for the count variations among pixels resulting from inter pixel gain and residual threshold dispersion variations. In this regard, the Medipix3RX is well known to feature a very good homogeneity between pixels [1]. The proposed inter pixel correction methods can be expected to yield significantly higher improvements in the overall energy resolution for detectors with more severe inter pixel variations, where a global energy calibration would be insufficient.

IV. Acknowledgements

The authors are thankful for discussions with several Medipix3 collaboration members at CERN.

References

[1] R. Ballabriga *et al.*, "The Medipix3RX: A high resolution, zero dead-time pixel detector readout chip allowing spectroscopic imaging," *J. Instrum.*, vol. 8, no. 2, p. C02016, 2013.

[2] R. Ballabriga *et al.*, "Review of hybrid pixel detector readout ASICs for spectroscopic X-ray imaging," *J. Instrum.*, vol. 11, no. 1, p. P01007, 2016.

[3] S. R. Amendolia *et al.*, "MEDIPIX: A VLSI chip for a GaAs pixel detector for digital radiology," *Nucl. Instrum. Methods Phys. Res. A, Accel. Spectrom. Detect. Assoc. Equip.*, vol. 422, nos. 1–3, pp. 201–205, 1999.

[4] J. Watt *et al.*, "Dose reductions in dental X-ray imaging using Medipix," *Nucl. Instrum. Methods Phys. Res. A, Accel. Spectrom. Detect. Assoc. Equip.*, vol. 513, nos. 1–2, pp. 65–69, 2003.

[5] L. Yu *et al.*, "Radiation dose reduction in computed tomography: Techniques and future perspective," *Imag. Med.*, vol. 1, no. 1, pp. 65–84, 2009.

[6] M. Åslund, B. Cederström, M. Lundqvist, and M. Danielsson, "Physical characterization of a scanning photon counting digital mammography system based on Si-strip detectors," *Med. Phys.*, vol. 34, no. 6, pp. 1918–1925, 2007.

[7] E. Fredenberg, M. Hemmendorff, B. Cederström, M. Åslund, and M. Danielsson, "Contrast-enhanced spectral mammography with a photon-counting detector," *Med. Phys.*, vol. 37, no. 5, pp. 2017–2029, 2010.

[8] H. Ding, H.-M. Cho, W. C. Barber, J. S. Iwanczyk, and S. Molloi, "Characterization of energy response for photon-counting detectors using X-ray fluorescence," *Med. Phys.*, vol. 41, no. 12, p. 121902, 2014.

[9] E. Roessl and R. Proksa, "K-edge imaging in X-ray computed tomography using multi-bin photon counting detectors," *Phys. Med. Biol.*, vol. 52, no. 15, p. 4679, 2007.

[10] R. E. Alvarez and A. Macovski, "Energy-selective reconstructions in X-ray computerised tomography," *Phys. Med. Biol.*, vol. 21, no. 5, p. 733, 1976.

[11] J. P. Ronaldson *et al.*, "Toward quantifying the composition of soft tissues by spectral CT with Medipix3," *Med. Phys.*, vol. 39, no. 11, pp. 6847–6857, 2012.

[12] Z. Yu *et al.*, "Evaluation of conventional imaging performance in a research whole-body CT system with a photon-counting detector array," *Phys. Med. Biol.*, vol. 61, no. 4, p. 1572, 2016.

[13] D. Gürsoy and M. Das, "Single-step absorption and phase retrieval with polychromatic X rays using a spectral detector," *Opt. Lett.*, vol. 38, no. 9, pp. 1461–1463, 2013.

[14] M. Das and Z. Liang, "Spectral X-ray phase contrast imaging for single-shot retrieval of absorption, phase, and differential-phase imagery," *Opt. Lett.*, vol. 39, no. 21, pp. 6343–6346, 2014.

[15] R. N. Wilke *et al.*, "High-flux ptychographic imaging using the new 55μm-pixel detector 'Lambda' based on the Medipix3 readout chip," *Acta Crystallographica A, Found. Adv.*, vol. 70, no. 6, pp. 552–562, 2014.

[16] K. Taguchi and J. S. Iwanczyk, "Vision 20/20: Single photon counting X-ray detectors in medical imaging," *Med. Phys.*, vol. 40, no. 10, p. 100901, 2013.

[17] T. G. Schmidt and F. Pektas, "Region-of-interest material decomposition from truncated energy-resolved CT," *Med. Phys.*, vol. 38, no. 10, pp. 5657–5666, 2011.

[18] H. Ding and S. Molloi, "Image-based spectral distortion correction for photon-counting X-ray detectors," *Med. Phys.*, vol. 39, no. 4, pp. 1864–1876, Apr. 2012.

[19] A. M. Alessio and L. R. MacDonald, "Quantitative material characterization from multi-energy photon counting CT," *Med. Phys.*, vol. 40, no. 3, p. 031108, 2013.

[20] N. R. Fredette, C. E. Lewis, and M. Das, "A multi-step method for material decomposition in spectral computed tomography," *Proc. SPIE, Phys. Imag.*, vol. 10132, 2017.
[21] T. Koenig *et al.*, "How spectroscopic X-ray imaging benefits from inter-pixel communication," *Phys. Med. Biol.*, vol. 59, no. 20, p. 6195, 2014.
[22] T. Koenig *et al.*, "Charge summing in spectroscopic X-ray detectors with high-Z sensors," *IEEE Trans. Nucl. Sci.*, vol. 60, no. 6, pp. 4713–4718, Dec. 2013.
[23] R. Ballabriga, M. Campbell, E. Heijne, X. Llopart, L. Tlustos, and W. Wong, "Medipix3: A 64 k pixel detector readout chip working in single photon counting mode with improved spectrometric performance," *Nucl. Instrum. Methods Phys. Res. A, Accel. Spectrom. Detect. Assoc. Equip.*, vol. 633, pp. S15–S18, May 2011.
[24] E. N. Gimenez *et al.*, "Characterization of Medipix3 with synchrotron radiation," *IEEE Trans. Nucl. Sci.*, vol. 58, no. 1, pp. 323–332, Feb. 2011.
[25] H.-M. Cho, H. Ding, B. P. Ziemer, and S. Molloi, "Energy response calibration of photon-counting detectors using X-ray fluorescence: A feasibility study," *Phys. Med. Biol.*, vol. 59, no. 23, p. 7211, 2014.
[26] R. K. Panta, M. F. Walsh, S. T. Bell, N. G. Anderson, A. P. Butler, and P. H. Butler, "Energy calibration of the pixels of spectral X-ray detectors," *IEEE Trans. Med. Imag.*, vol. 34, no. 3, pp. 697–706, Mar. 2015.
[27] M. Das, B. Kandel, C. S. Park, and Z. Liang, "Energy calibration of photon counting detectors using X-ray tube potential as a reference for material decomposition applications," *Proc. SPIE, Phys. Imag.*, vol. 9412, 2015.
[28] K. Taguchi, E. C. Frey, X. Wang, J. S. Iwanczyk, and W. C. Barber, "An analytical model of the effects of pulse pileup on the energy spectrum recorded by energy resolved photon counting X-ray detectors," *Med. Phys.*, vol. 37, no. 8, pp. 3957–3969, Aug. 2010.
[29] E. Frojdh *et al.*, "Count rate linearity and spectral response of the Medipix3RX chip coupled to a 300μm silicon sensor under high flux conditions," *J. Instrum.*, vol. 9, no. 4, p. C04028, 2014.
[30] *NIST XCOM Data*. Accessed: Mar. 20, 2017. [Online]. Available: https://physics.nist.gov/PhysRefData/Xcom/html/xcom1.html
[31] Y. Ge, X. Ji, R. Zhang, K. Li, and G.-H. Chen, "K-edge energy-based calibration method for photon counting detectors," *Phys. Med. Biol.*, vol. 63, no. 1, p. 015022, 2017.
[32] J. S. Lee, D.-G. Kang, S. O. Jin, I. Kim, and S. Y. Lee, "Energy calibration of a CdTe photon counting spectral detector with consideration of its non-convergent behavior," *Sensors*, vol. 16, no. 4, p. 518, 2016.
[33] R. W. Schafer, "What is a savitzky-golay filter? [lecture notes]," *IEEE Signal Process. Mag.*, vol. 28, no. 4, pp. 111–117, Jul. 2011.

Robust Energy Calibration Technique for Photon Counting Spectral Detectors

Stefano Vespucci, Chan Soo Park, Raul Torrico, and Mini Das

***Abstract*— This paper describes the implementation of a novel and robust threshold energy calibration method for photon counting detectors using polychromatic X-ray tubes. Methods often used for such energy calibration may require re-orientation of the detector or introduce calibration errors that are flux and acquisition time-dependent. Our newly proposed "differential intensity ratios" (DIR) method offers a practical and robust alternative to existing methods. We demonstrate this robustness against photon flux used in calibration, spectral errors such as pulse pile-up as well as the detector's inherent spectral resolution limits. The demonstrated significant insensitivity of the proposed DIR signature to detector spectral distortions and energy resolution is a key finding. The proposed DIR calibration method is demonstrated using Medipix3RX detectors with a CdTe sensor under varying flux conditions. A per pixel calibration using the DIR method has also been implemented to demonstrate an improvement over the global energy resolution of the PCD.**

***Index Terms*— Energy calibration, photon counting detectors, x-ray detector, spectral resolution, x-ray fluorescence, Medipix.**

I. Introduction

SEMICONDUCTOR quantum detectors capable of resolving and processing single photons are emerging as powerful tool for many imaging applications. Recent versions of these single photon counting detectors (PCDs) are capable of energy discrimination and intercommunication between pixels to reduce spectral distortions [1], [2]. Besides spectral discrimination, PCDs allow image acquisition with zero dark noise resulting in an improved image quality with the potential for several low-dose medical and biological application [3]–[7]. These common imaging techniques include x-ray fluorescence (XRF) [8], K-edge absorption [9], computerized tomography (CT) [10]–[12], phase contrast [13], [14], ptychography [15] and material decomposition techniques [16]–[20].

PCDs are direct conversion detectors that use semiconductor sensors to convert x-rays to charge clouds. Electronic discriminators allow a comparison of signal generated by the incident photons with internal electronic threshold values. These values are commonly denoted as "thresholds" for the PCD. This mechanism allows filtering of photons that have energies lower than that corresponding to the electronic threshold chosen by the experimenter. Energy calibration is a process of accurately assigning the energy value corresponding to an electronic threshold corresponding to a particular digital-to-analog converter (DAC) value. This energy calibration of PCD thresholds is a required procedure before effectively using the spectral capabilities of these devices.

A global energy calibration, performed for all the pixels in the PCD, may be sufficient for many applications. It determines the average energy response of all the pixels in the PCD. The inter-pixel manufacturing variations in the detector electronics (like threshold and gain variations) lead to slight differences in energy calibration between pixels [1], [21] This results in a globally reduced energy resolution in the PCD. By evaluating the energy response of each pixel independently, a significant improvement in the energy resolution can be achieved.

Electronic settings such as pixel gain or current levels within the detector require separate optimization based on a particular application. One must also ensure robustness of spectral response due to temperature sensitivity or unforeseen effects of slow radiation damage to the electronics. Thus a routine PCD calibration to check for stable spectral response is desirable. Fast, simple and robust methods would be required for routine calibrations when these detectors are used in a clinical setting in the future. Most existing energy calibration techniques are influenced by the detector's intrinsic resolution, which decreases with increasing energy. In this paper, we present a robust energy calibration method that overcomes these limitations. Aspects such as robustness of calibration techniques to varying acquisition times and to flux changes are also addressed. While the methods discussed in this paper are relevant to any photon counting detector, we demonstrate the proposed methods using Medipix3RX detector with a CdTe sensor. We also demonstrate the utility of our proposed method for per pixel calibration with improved spectral data.

A. Medipix3RX Detector

The Medipix3RX detector [1], [21], [22] is a direct conversion semiconductor hybrid pixel detector developed by an international collaboration based in CERN, Geneva. It has

Manuscript received August 3, 2018; revised September 29, 2018; accepted October 7, 2018. This work was supported in part by the U.S. Department of Defense (DOD) Congressionally Directed Medical Research Program (CDMRP) Breakthrough Award under Award BC151607 and in part by the National Science Foundation CAREER Award under Award 1652892. *(Corresponding author: Mini Das.)*

The authors are with the Department of Physics, University of Houston, Houston, TX 77204 USA (e-mail: mdas@central.uh.edu).

Color versions of one or more of the figures in this paper are available online at http://ieeexplore.ieee.org.

Digital Object Identifier 10.1109/TMI.2018.2875932

spectroscopic capabilities allowing up to eight electronic thresholds to be used for energy discrimination.

Medipix3RX detector consists mainly of two parts: the sensor, where the incoming photons are converted into electron-hole pairs, and the Medipix3RX application specific integrated circuit (ASIC) electronics, where the signal is processed for readout. The sensor is usually a semiconducting material such as Si, CdTe or GaAs and consists of a diode structure. A grid of equally spaced metallic bump-bonds behind the sensor allows for virtual pixellation. Each bump-bond is connected to the ASIC electronics, allowing for independent readout for every pixel.

A reverse bias voltage is applied to the sensor in order to deplete the diodes junction interface region and to create an electric field within the sensor. This voltage depends on a number of factors such as sensor material, sensor thickness and doping concentration within the sensor. The electric field allows the generated charge cloud to drift toward the ASIC electronics, where the signal is processed. The incident x-ray photons generate charge cloud, which is then collected at the electrode and readout for each pixel. The external electric field helps to minimize the lateral diffusion of charge cloud, thereby reducing charge sharing effects. Critical spectral errors can result if the charge cloud is partially collected by the neighboring pixels and read erroneously as a low-energy photon [23], [24].

The Medipix3RX detector unit has an active area that is composed of 256 $\times$ 256 pixels, each measuring 55 $\mu m \times$ 55 μm. The various operating modes for Medipix3RX can be found in prior literature [1], [2], [23], [24]. The charge summing mode allows one to utilize the built-in correction for charge sharing via inter-pixel communication enabled in the hardware [1]. This is a desirable mode for most of our applications due to improved spectral fidelity. For Medipix3RX, one can further choose a fine-pitch mode that allows the highest spatial resolution of 55 μm which is also desirable for many of our applications. Hence the energy calibrations shown in this paper are done in a fine pitch mode with charge sharing correction.

For a selected DAC threshold value, the detector pixels count the number of photons having an energy above that of the energy E_i represented by the selected threshold. For any given threshold energy E_i, the integral mode count ($I^{int}(E_i)$) is:

$$I^{int}(E_i) = \int_{E_i}^{\infty} \Phi(E) D(E) dE, \qquad (1)$$

where $\Phi(E)$ is the spectrally dependent incident x-ray flux and $D(E)$ the detector response function, which takes into account factors such as absorption efficiency, flux dependence and spectral distortions like charge sharing and pile-up.

A common operation which is performed in order to monitor the spectral energy response of the detector as a function of the digital-to-analog-converter (DAC) threshold value is referred to as the threshold DAC scan. Here the photons collected for each DAC threshold is recorded (for a selected time interval) as the threshold value is systematically incremented at finite intervals. As seen in Eq. 1, this data represents the integral of counts above a given threshold as we vary the threshold level during the scan. This integral-mode spectra has to be differentiated to obtain the photon counts corresponding to each threshold (or the corresponding energy) referred to as differential mode spectra in this paper.

Accurate energy calibration (deciphering what the corresponding energy is for each threshold) requires known sources of x-ray emission or absorption to be used as sharp reference points. With at least three reliable measurements, a threshold-energy calibration curve can be obtained, which then allows one to match any arbitrary threshold to the corresponding x-ray energy. Some reference energy sources used are radioactive sources, x-ray fluorescence sources [25], peak x-ray source emission (referred to as kVp calibration) [26], [27] and K-edge of any given material. Some drawbacks of these methods are the following: low count rates when using radioactive source emissions as reference; the need for re-orienting the detector when using metal fluorescence lines for reference (as shown in Sec. II-B1); the flux-dependent drifting of calibration curve when using a kVp method (as shown in Sec. II-B3); the broadening of absorption edge due to limited detector spectral resolution when using K-edge absorption method (as shown in Sec. II-B2). In Sec. II-C we describe a robust calibration method against source flux and the limited detector inherent resolution. An x-ray fluorescence method (described in Sec II-B1) is used as a gold standard to compare our new approach. While XRF method requires re-organizing the imaging setup and time consuming, the results obtained are fairly robust due to the relatively low count rate. The presence of a sharp emission peak also offers accuracy in spite of the spectral broadening due to the detector resolution.

II. Experimental Methods

A. Medipix3RX Measurement Setting

All the experiments reported in this paper are performed by using a micro-focus x-ray tube L8121-03 from Hamamatsu with a Tungsten anode and with operating limits of up to 150 kV and 500 μA. The Medipix3RX detectors with 1000 μm thick CdTe sensor was used, with an applied bias voltage of $-$500V to the sensor. An equalization for threshold dispersion among pixels were performed prior to the measurements. This operation fine tunes the thresholds in each pixel within the matrix to enable improved inter pixel response uniformity.

For each detected photon, the pixel electronics require a finite time to collect and process the signal. The pixel remains in an inactive state for this interval of time (called the dead time, τ) leading to what is known as a dead-time loss [28]. Hence, quasi-coincident photons may be recorded as a single event for high flux-rates. The result is an apparent reduction in the photon counts and a distortion of the measured energy spectrum due to pulse pile-up [28]. The magnitude of spectral distortion due to pile-up is proportional to the incident flux rate [28].

The detector dead time was estimated by fitting the measured flux rates to an analytical paralyzable model [22], [24] (see Eq. 2) for a range of photon fluxes obtained by changing

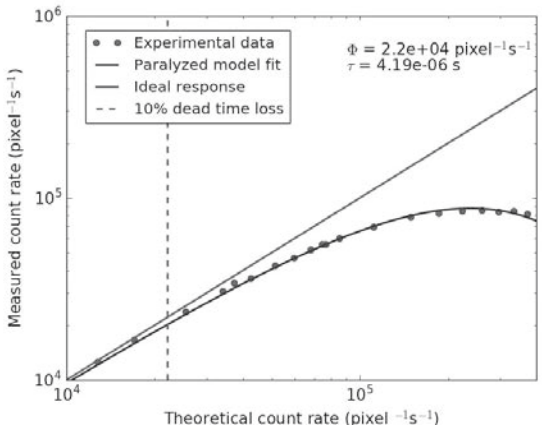

Fig. 1. Measured photon fluxes as function of the expected fluxes for a paralyzable model. The vertical dashed line shows the position of the 10% dead time loss for Medipix3RX CdTe detector.

the source detector distances.

$$\Phi_{meas} = \Phi_{est} e^{-\Phi_{est}\tau}, \tag{2}$$

where Φ_{meas} and Φ_{est} are the measured and estimated photon fluxes per pixel respectively, given in unit of s^{-1} and τ is the pixel dead time in seconds. Φ_{est} is extrapolated from experimental data measured at very low count rates when pile up effect is negligible.

Fitting the data acquired at increasing x-ray flux rates to this paralyzable model (Figure 1) yielded a dead time of 4.2 μs for the Medipix3RX detector with a 1000 μm thick sensor. This value is comparable with what is found in the literature [29] for similar detector settings. Flux rate levels used for the experiments in this paper range from $\approx$ 43 counts/s/pixel to $\approx 1.5 \times 10^5$ counts/s/pixel. Pile-up effects might be considered limited only for photon flux values below $\approx 2.5 \times 10^4$ counts/s/pixel, resulting in at least 10% dead time loss (shown by vertical dashed line in Fig. 1).

B. Existing Calibration Techniques

A number of existing energy calibration methods were tested and compared against our newly proposed method (Sec.II-C).

1) X-Ray Fluorescence: X-ray fluorescence (XRF) emission peaks from metals can be used as references for energy calibration of PCDs. Since XRF signal is low compared to the primary x-ray beam, for these measurements, the detector is positioned at 90° with respect to the target and the primary beam (Fig. 2(a)).

The x-ray source was operated at 250 μA and 100 kV. The threshold scans were performed for all targets by using an acquisition time of 1 s per frame, and varying the DAC threshold from 20 to 150, using a step size of one DAC threshold (corresponding to $\approx$ 1 keV). The values of $K_{\alpha 1}$, $K_{\alpha 2}$ and K-edge (corresponding to K shell electron binding energy) from the elements used for our XRF and K-edge calibration are listed in Table I. The resulting XRF calibration line is shown in Fig. 3.

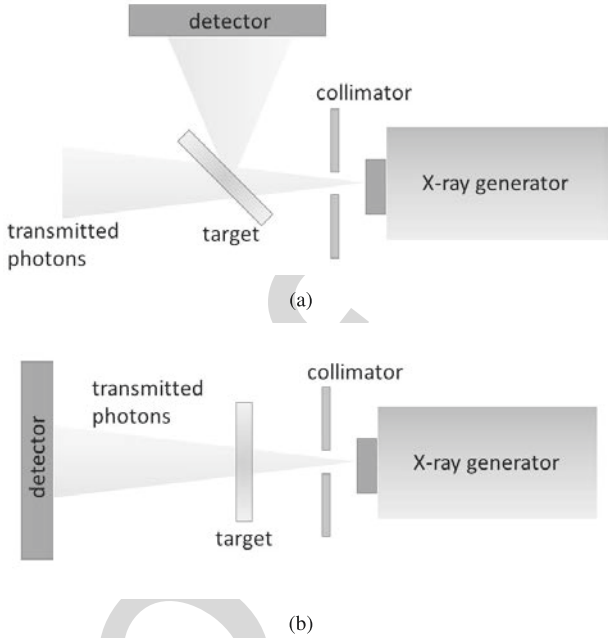

Fig. 2. Sketch showing the experimental set up used for (a) XRF and (b) K-edge absorption measurements.

TABLE I
LIST OF THE ELEMENTS USED FOR XRF CALIBRATION AND CORRESPONDING $K_{\alpha 1}$, $K_{\alpha 2}$ AND K-EDGE EMISSION VALUES [30]

Element	$\mathbf{K_{\alpha 1}}$ **(keV)**	$\mathbf{K_{\alpha 2}}$ (keV)	**K-edge** (keV)
Zr	15.77	15.69	18.00
Sn	25.27	25.04	29.21
Nd	37.36	36.85	43.57
Gd	43.00	42.31	50.21
W	59.32	57.98	69.52
Pb	75.00	72.80	88.01

Energy resolution (ΔE) can be indicated in terms of the full width at half maximum (FWHM). By using K_α emission peaks from target materials ΔE, and the relative energy resolution ($\frac{\Delta E}{E}$), was measured at energies corresponding the XRF K_α from Zr, Gd, W and Pb (showing well defined Gaussian peaks). These are shown in Fig. 3 (b - c) respectively.

Due to the need for re-arranging the detector, XRF calibrations may not be accessible in a PCD CT system. However energy calibrations using XRF is very precise and reliable. For this reason, we use the energy calibration from XRF as reference for all the other calibration methods. In the remaining sections of this paper, all the threshold values are expressed in energy units based on the corresponding XRF calibration.

2) K-Edge Absorption: Threshold calibration using K-edge absorption uses a simple transmission geometry (Fig. 2(b)). The energy dependent attenuation coefficients of target material are measured and the K-absorption edge is used as reference in the calibration. The linear absorption coefficient measured from a W plate (0.1 mm thick) as a function of varying energy is shown in Fig. 4. This data was acquired by scanning the energy threshold from $\approx$ 20 keV to $\approx$ 120 keV,

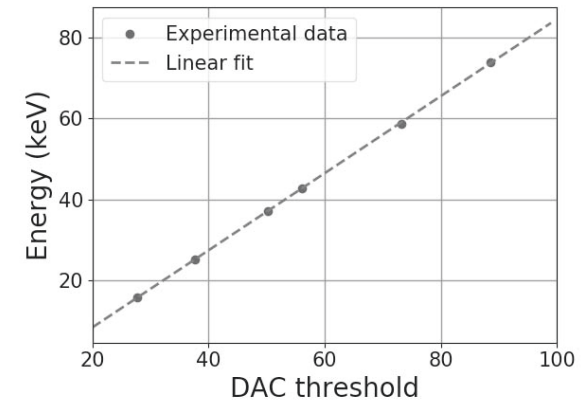

(a)

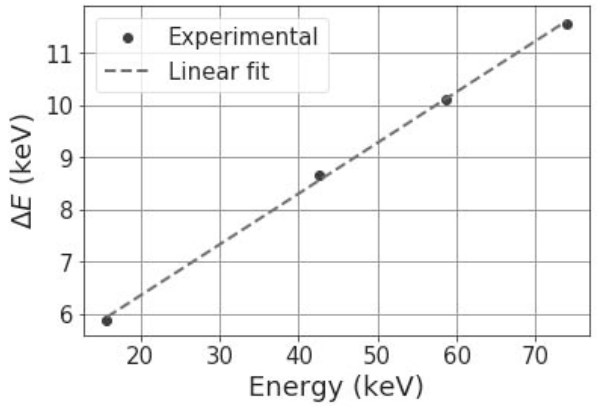

(b)

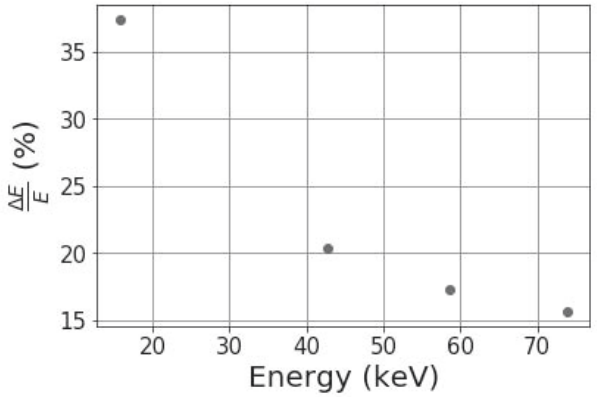

(c)

Fig. 3. (a) Threshold energy calibration obtained for the Medipix3RX chip having a CdTe 1000 μm thick sensor, using K_α XRF emissions from the elements listed in Table I. (b) Energy resolution (FWHM) and (c) relative energy resolution ($\frac{\Delta E}{E}$) measured from Zr, Gd, W and Pb targets.

using a threshold step equivalent of $\approx$ 1 keV. The energy values shown on x-axis correspond to the respective thresholds (based on XRF calibrations in Sec. II-B1). For reference, the K-edge energy (69.52 keV) of the W target is shown with a vertical dashed line (obtained from the NIST database [30]). As observed, due to the limited energy resolution of the detector as well as the non-ideal and flux dependent detector spectral response, the measured transitions at the characteristic

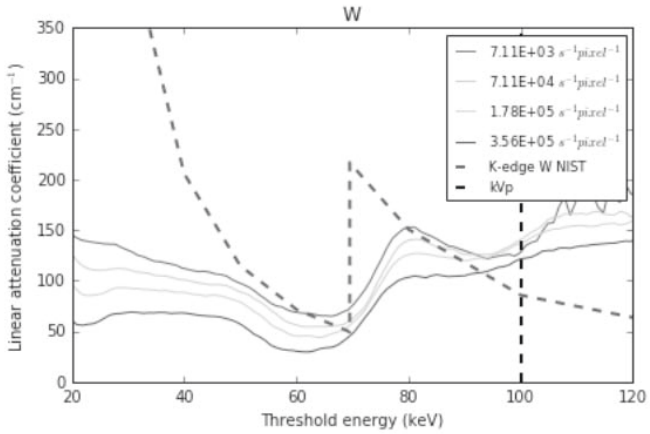

Fig. 4. Linear attenuation coefficient measured from a W target.

K-edge energies are quite broad. Hence it is difficult to precisely determine the DAC threshold value corresponding to the K-edge energy, making it a challenge to use this method for energy calibration [31]. Fig. 4 also shows the strong spectral distortion introduced by the detector for energies well below the K-edge as well as near the kVp.

A strategy to mitigate these issues due to the limited detector energy resolution is described in Sec. II-C.

3) X-Ray Tube Voltage Peak: Peak voltages (kVp) corresponding to the x-ray tube spectra has shown to be useful references for energy calibration of PCDs [26], [27], [32]. These reference points correspond to the maximum energy for photons emitted from a polychromatic x-ray tube for a set acceleration voltage [26], [27], [32]. One advantage of this method is the continuous range of energies available from the x-ray tube and the simple setup requiring no additional hardware or target materials.

The method is based on the determination of the highest energy (and corresponding threshold) at which all the pixels in the detector detect zero photons, which should occur at the tube kVp. However, since the energy response of pixels in the matrix have a normal distribution, such a sharp cut off is not seen. During a threshold scan about 50% of the total pixels in the detector would count at least one photon at the DAC threshold corresponding to the peak energy of the x-ray spectrum [26]. This threshold value for which 50% of pixels are ON can be treated as the reference for the peak tube voltage (kVp) [26], [27].

By repeating this procedure for a number of kVp values for which the x-ray tube can be turned on sequentially, a calibration line can be obtained [26], [27]. Although the kVp method provides quick results, a number of non-converging behaviors have been reported [27], [32] and observed by the authors in our own laboratory. The calibration curve shifts with varying exposure times and changing flux. This effect has been explained in terms of stochastic noise building up over the time. Sources of noise can be for example thermal noise or pile-up effects [32].

We tested this divergence from ideal behavior for various flux conditions obtained by changing tube currents to 50 μA, 100 μA, 150 μA, 250 μA and 350 μA for a set source to

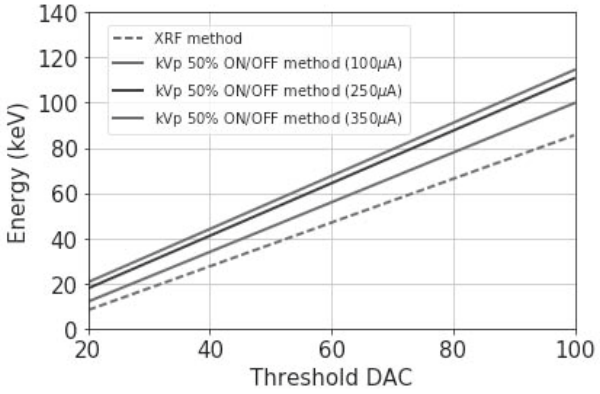

Fig. 5. Comparison between calibration lines obtained by applying the kVp method on dataset obtained using three x-ray tube currents (100, 250 and 350 μA) and the standard XRF method.

detector distance of 46 cm. For each current value, a range of x-ray source peak voltages were used, from 25 kVp to 125 kVp with a step of 25 kV to get a calibration line corresponding to each flux rate determined by the tube current (see Fig. 5).

Figure 5 shows three calibration lines, obtained by applying the kVp method to three flux levels by operating at x-ray tube currents, 100 μA, 250 μA and 350 μA respectively. The XRF based calibration is shown for comparison as well. Strong dependence of calibration on photon flux is evident. A deviation of up to 30 keV can be observed for even a photon flux that is well below the 10% dead time loss flux rate. The flux levels in clinical CT systems are much higher than what is used in our benchtop system and much larger deviations and uncertainty in calibrations could be expected. The newly proposed calibration method in this paper (Sec. II-C) are aimed for improved robustness against photon flux used during calibration in kVp method. The following sections describe the DIR method as applied to both kVp and K-edge type calibration methods for a PCD.

C. Differential Intensity Ratios Method

The method is based on our observation that the differential or relative variations in photon counts is significantly sharper than the actual variation of counts at the K-absorption edge as well as at the peak energy of the x-ray spectrum (kVp). The method is summarized below for a general case when a K-edge material is used for reference with specific examples presented in subsequent sections. First, the energy dependent integral mode photon counts at the detector is measured with and without the target material placed between the x-ray tube and the detector (setup shown in Fig. 2(b)). For each threshold ($i = 1, 2, \ldots$), a spectrally varying intensity I^{int} and I_0^{int} is obtained with and without the target. The intensity data acquired in integral mode using the Medipix3RX can be described as:

$$I^{int}(E_i) = \int_{E_i}^{\infty} \Phi(E) e^{-\mu(E)x} D(E) dE \tag{3}$$

$$I_0^{int}(E_i) = \int_{E_i}^{\infty} \Phi(E) D(E) dE, \tag{4}$$

where $\Phi(E)$ is the incident x-ray spectrum, $\mu(E)$ and x are the linear attenuation coefficient and thickness of the target and $D(E)$ is the detector response function which includes flux dependence. I^{int} and I_0^{int} represent the target data and the flat field data respectively.

The energy spectrum is obtained by differentiating the integral data with respect to the discrete threshold values:

$$I_i = \frac{I_i^{int} - I_{i+\Delta i}^{int}}{\Delta i} \tag{5}$$

$$= \int_{E_i}^{E_{i+\Delta i}} \Phi(E) e^{-\mu(E)x} D(E) dE \tag{6}$$

$$I_{0,i} = \frac{I_{0,i}^{int} - I_{0,i+\Delta i}^{int}}{\Delta i} \tag{7}$$

$$= \int_{E_i}^{E_{i+\Delta i}} \Phi(E) D(E) dE \tag{8}$$

A flat field correction, e.g. the division between data acquired with the target and the data acquired without the target,

$$\frac{I_i}{I_{0,i}} = \frac{\int_{E_i}^{E_{i+\Delta i}} \Phi(E) e^{-\mu(E)x} D(E) dE}{\int_{E_i}^{E_{i+\Delta i}} \Phi(E) D(E) dE} \tag{9}$$

$$\simeq \left\langle e^{-\mu(E)x} \right\rangle_i, \tag{10}$$

is performed for each threshold. If the flux difference with and without the target is very large leading to change in detector response functions, the D(E) values in the numerator and denominator of Eq. 9 would only approximately be the same. This approximation is noted in Eq. 10. Finally, the flat field corrected intensities can be differentiated with respect to the applied threshold,

$$DIR = -\frac{\partial}{\partial i} \frac{I_i}{I_{0,i}}. \tag{11}$$

The trend of DIR would reveal Gaussian-like peaks at K-edge energies for the target material and at the kVp of x-ray tube spectrum. These observed peaks can be used as references to find energies corresponding to the electronic thresholds. By using multiple K-edge materials in the beam path simultaneously, one can acquire a calibration line in a single shot. The K-edge from high energy efficient sensor material (e.g. Cd and Te) can also be often used as a reference point.

The newly proposed calibration method was applied to the experimental dataset acquired from K-edge experiments described previously in section II-B2.

Figure 6(a) shows threshold scans acquired in integral mode by monitoring the photons transmitted through a Gd target, see Eq. 3. In order to compare threshold scans acquired under different photon flux conditions, counts displayed in the figure were normalized by the total number of photon counts for the entire scan.

Figure 6(b) shows the corresponding differential mode data with flat field correction. This data corresponding to $\frac{I_i}{I_{0,i}}$ (see Eq. 9) shows three distinct transitions. Two of these peaks are at K-edge energies corresponding to Cd (26.7 keV, from the CdTe sensor) and to Gd target (50 keV). The third peak is from the peak energy (100 keV) corresponding to the

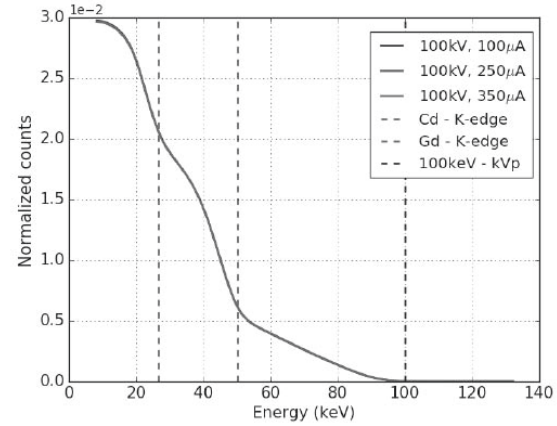

(a)

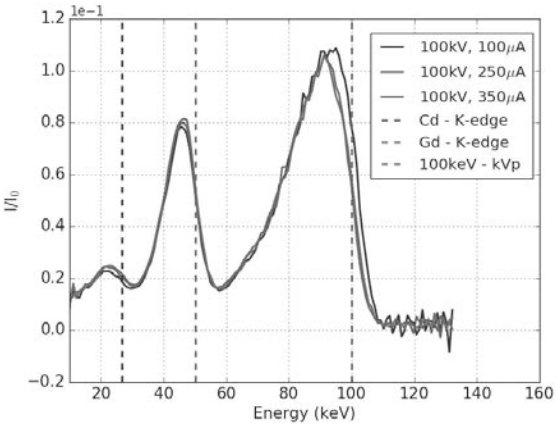

(b)

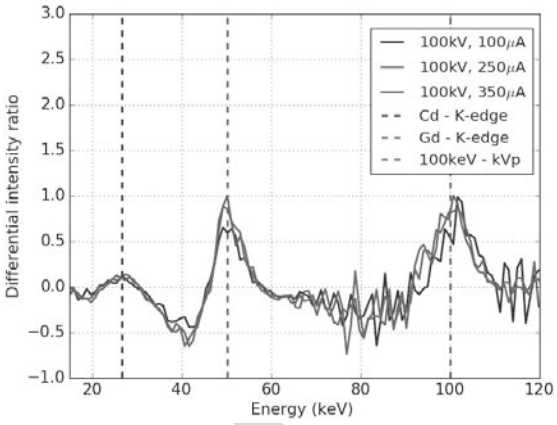

(c)

Fig. 6. Results from the new implemented method from Gd. (a) Threshold scans (see Eq. 3); (b) division between I and I_0 (see Eq. 9) (c) differential intensity ration (see Eq. 11).

x-ray spectrum. These reference energies are highlighted by vertical dashed lines in red, green and blue respectively in Fig. 6(a-c). Figure 6(c) shows the DIR plot (see Eq. 11) following the differentiation operation applied to the data shown in Fig. 6(b). The noise seen in this data is a result of differentiation. A smoothing operation can resolve this noise effectively (shown later in Fig. 8).

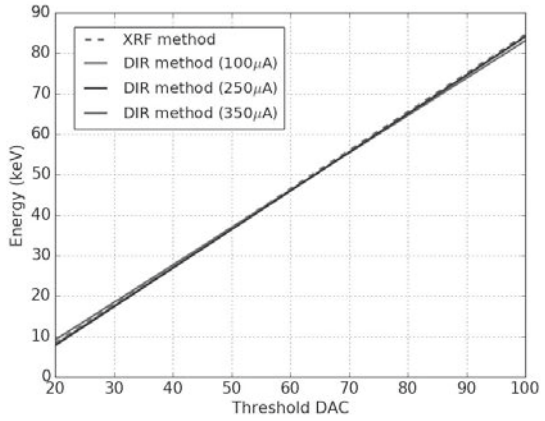

Fig. 7. Comparison between calibration lines obtained by applying DIR and XRF methods.

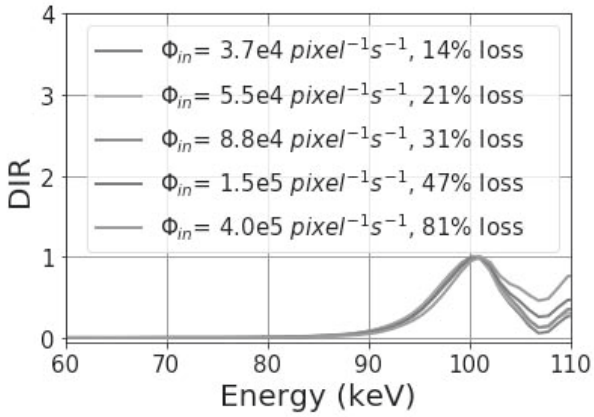

Fig. 8. Peaks obtained by applying the proposed method to dataset obtained using a x-ray tube peak voltage of 100kVp and different photon fluxes.

The peaks are clearly visible at all the three characteristic energies in Fig. 6(c). The DAC threshold corresponding to the characteristic energies is obtained via a Gaussian fit. In order to have additional data points, the procedure was also repeated for the W target (K-edge at 70 keV) in the beam path, and a calibration line was obtained. The position of the peaks in Fig. 6(c) appear to be negligibly dependent on the x-ray tube current value, at least for the range of currents used in our experiments. A comparison between the XRF and DIR calibration lines obtained using different x-ray tube current values is shown in Fig. 7. Please note that the energy resolution of PCD is not improved by applying the DIR method. The advantage, compared to conventional absorption measurements is that the DIR approach localizes the point where the K-edge transition occurs thus allowing a more accurate and robust energy calibration for the detector. Spectral inaccuracies due to calibration can add to the effects of distortions when collecting spectral data using PCDs.

Although the DIR peak seen at the characteristic K-edge energies are clearly related to a property of the target material,

i.e. the DIR peak is the result of the sudden change in the signal occurring at the K-edge, the peak found at the kVp energy is not. It is possible, indeed, to reveal a kVp DIR peak by applying the DIR method to any two dataset acquired under different photon fluxes and with no target material in the beam path. This is described more in detail in the next section. This observation suggests that the origin of the kVp peak has to be attributed to the detector response, D(E), which is flux dependent [28].

D. Robustness of the DIR Method Against Photon Flux

In order to examine the use of DIR method solely to kVp references, we applied the proposed procedure only to the flat field threshold scans (no target in the beam path) obtained at two different tube currents. In this case Eq. 11 can be re-written as:

$$DIR = -\frac{\partial}{\partial i}\frac{I_{0,i}^{ref}}{I_{0,i}^{n}}, \tag{12}$$

where $I_{0,i}^{ref}$ and $I_{0,i}^{n}$ are any two dataset acquired with the same experimental conditions but different x-ray tube currents. Furthermore, in order to demonstrate the robustness of the method against the photon flux, a range of photon fluxes were used, this time well above the 10% dead time loss. Flux rates of 1.9×10^3, 3.7×10^4, 5.5×10^4, 8.8×10^4, 1.5×10^5 and 4.0×10^5 counts pixel^{-1}s^{-1}, corresponding to dead time losses of 0.8%, 14%, 21%, 31%, 47% and 81% were used.

In our case, $I_{0,i}^{ref}$ consisted of the dataset acquired under the lowest flux (1.9×10^3 counts pixel^{-1}s^{-1}). $I_{0,i}^{n}$ consisted of the datasets acquired using other larger flux rates. In order to eliminate high frequency differentiation noise (see Fig. 6), data were first smoothed by using a Savitzky-Golay filter, showing peak shape preservation properties [33].

The result of this experiment (shown in Fig. 8) confirms that the peak positions from DIR do not change significantly with the incident photon flux, demonstrating the excellent stability of this method against variations in the photon flux.

A possible explanation for the origin of the kVp DIR peak is the following. While the true photon counts would diminish to zero above the x-ray kVp (see Fig. 6(a)), the peak shown in the DIR is only the result of differential distortions in the spectrum due to variations in PCD response to flux. This can be possibly attributed to effects such as pulse pile up that are not immediately visible from spectral measurements at low fluxes (such as in Fig. 6(a) and Fig. 9(a) below. Figure 9(a) shows two normalized flat field energy spectra, acquired with photon fluxes below 10% dead time losses, where pile up effects are limited. Ideally, normalized datasets not affected by pile up spectral distortion should appear identical. At first glance, indeed, energy spectrums shown in Fig. 9(a) appear very similar to each other. However, upon closer look, Fig. 9(a) (see inset showing the zoom-in plot for energy around 100 keV) shows higher counts above the kVp (indicated by the vertical black dashed line) for the dataset acquired with higher flux. Such a difference between spectrums is enhanced by the division step of the DIR method, as shown in Fig. 9(b). There is an energy range where the two spectrums are not significantly different (i.e. their ratio is close to unity, as indicated by the horizontal red dashed line). At energy range around the kVp, instead, the division shows a peculiar s-shaped transition, indicating a sudden change in the

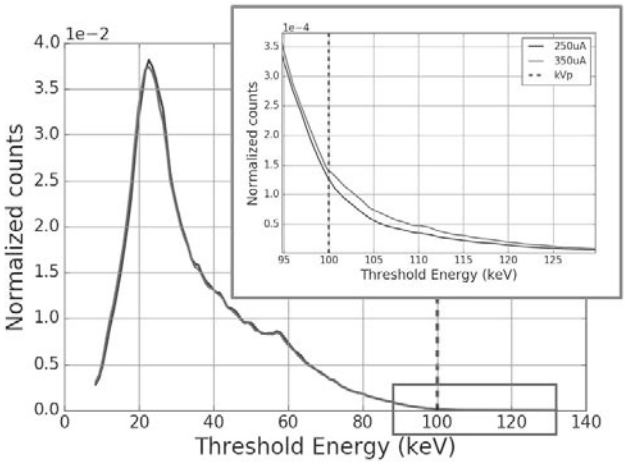

(a)

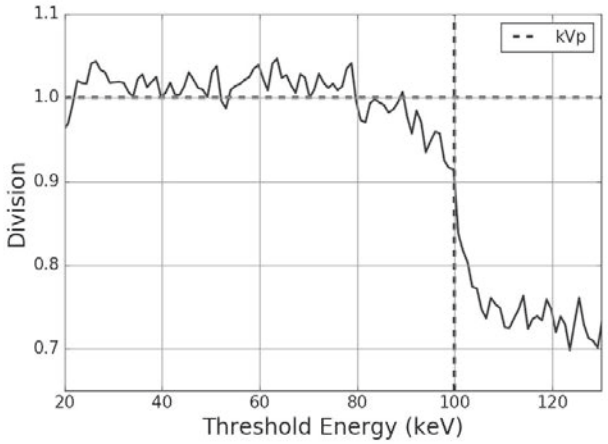

(b)

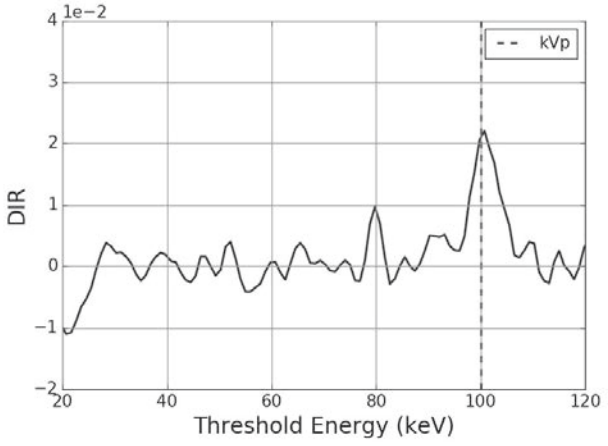

(c)

Fig. 9. DIR method applied to low flux flat field images. (a) Normalized energy spectrums highlighting dataset differences at the kVp energy; (b) ratio between datasets and (c) DIR peak at the kVp.

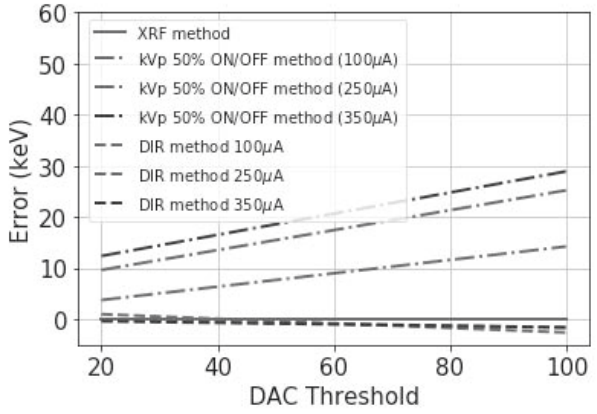

Fig. 10. Comparison between calibration methods. Discrepancy between DIR and kVp calibration methods and the XRF.

TABLE II
COMPARISON BETWEEN THE DEVIATION OF THE PRESENTED METHODS FROM THE XRF CALIBRATION LINE

RMS deviation from the XRF calibration (keV)		
	kVp method	DIR
100 μA	9.45	1.31
250 μA	17.99	0.99
350 μA	21.19	1.05

spectral distribution for this ratio at the kVp energy. The DIR peak seen at the kVp, shown in Fig. 9(c), directly reflects such a sudden transition. Thus while changes due to pile up effect are not visible for most of the spectra, it becomes relevant in the spectral ratio obtained in DIR (and hence the spectral change with changing flux). This can be clearly seen at and immediately after the kVp energy as the only photons detected after that energy is due to pile up effect.

E. Comparison of Calibration Methods

A comparison of global calibration lines obtained with the previously presented methods is shown in Fig. 10. The deviations from XRF based calibrations against the original kVp method [26], [27], [32] and DIR calibration method under various flux conditions is represented as errors (in keV).

As seen in Fig. 10, throughout the full range of thresholds and fluxes used in our studies, the calibration lines obtained using the DIR method remains very stable. However, the calibration lines obtained using the 50% ON-OFF kVp method leads to significant divergence when a high flux is used. In the worse case it is of the order of 30 keV. A summary is shown in Table II, where the root mean square (RMS) deviation from the XRF calibration, for the different methods is shown. As seen, the maximum divergence (less than 3 keV) due to changing flux in DIR is well within the detector's inherent resolution.

We can deduce that the conventional kVp method is only applicable when a relatively low x-ray tube current is used, and the range of applicability should be evaluated beforehand, for example using the method suggested by Lee *et al.* [32]. Working at very low flux levels can lead to very long durations for the calibration. The safe choice of highest flux is difficult to decide *a priori* as this may vary with sensor type, thickness and other factors. The kVp method is also more sensitive to random stochastic variations in the detector count and to pile-up effects. Our proposed DIR method shows stability and accuracy with respect to change in the incident photon flux, when compared to the conventional kVp method. It appears to be unaffected by the flux ranges used in our experiments.

F. Per Pixel Calibration and Correction Method

In the studies described above (Sec. II-C and II-D), the DIR method was applied to a global threshold calibration. An improvement in the overall energy resolution of the detector can be obtained by applying the same method to each pixel independently. This would significantly minimize the effect of pixel to pixel variations (pixel gain variations and residual threshold variations). For measurements using Medipix3RX, the DAC TH is a unique global variable which can be controlled by the user and this value represents the global threshold for all the pixels. For a chosen global DAC TH, the corresponding energy is obtained by using the global calibration line, which is of the form:

$$\overline{E} = m_{glob} \times TH + c_{glob}, \tag{13}$$

where m_{glob} and c_{glob} are slope and intercept of the global calibration line respectively. Equation 13 represents the average energy calibration line for all the pixels in the detector when the global DAC TH is varied.

Although the threshold equalization procedure (see Sec. II-A) minimizes the pixel to pixel variations by introducing a threshold offset in each pixel, it does not correct for the gain variations existing between pixels. Effectively, this means that for a chosen global threshold TH during any measurement, the true energy calibration line equation is slightly different for each pixel in the detector and can be given by

$$E_p = m_p \times TH + c_p, \quad p = 1, 2, 3, \ldots, N \tag{14}$$

where m_p and c_p are the slope and the intercept of the calibration line for each pixel p respectively.

In order to obtain the true calibration line for each pixel in the detector, one can simply apply the DIR method (described in II-C) to each pixel independently after masking off any bad pixels. From variation in slope of these individual calibration lines, the pixel gain (keV/threshold DAC) variations across the matrix can be estimated. The spatial distribution of pixel gain within the chip and the corresponding histogram for our detector is shown in Fig. 11(a-b) respectively. The gain variations across the pixel matrix, expressed as the standard deviation of the slopes of the calibration lines, results to be of the order of 0.05 keV/threshold DAC. The coefficient of variation $\frac{\sigma}{\mu}(\%)$, is equal to 5.4%. Here μ and σ are the mean value and the standard deviation of the pixel gains across the pixel matrix.

Once the energy response of each individual pixel is determined, correction schemes can be applied for any particular measurement. One possible implementation is described below.

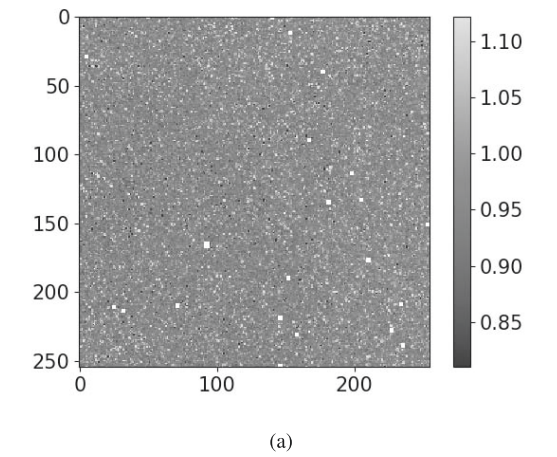

(a)

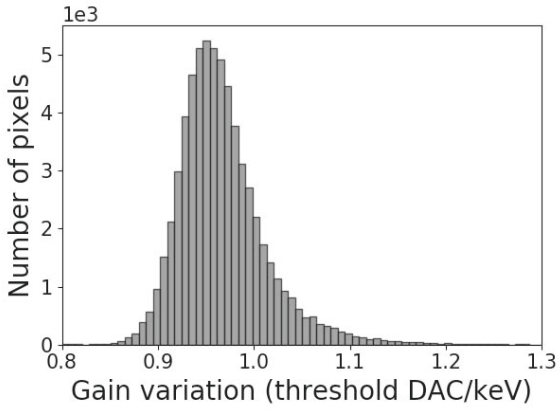

Fig. 11. Pixel gain variation across the PCD. (a) Spatial distribution of the gain and (b) corresponding histogram.

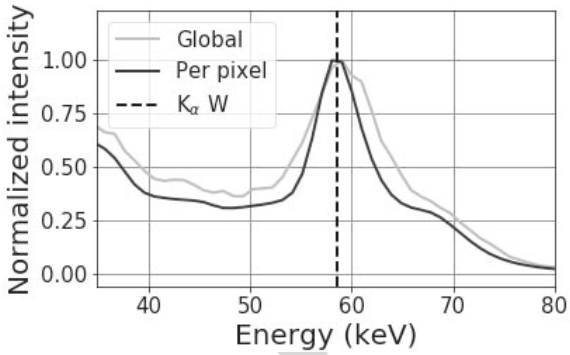

Fig. 12. Comparison between global and per pixel energy calibration. Correction procedure has been demonstrated using the K_α XRF peak recorded from a W target.

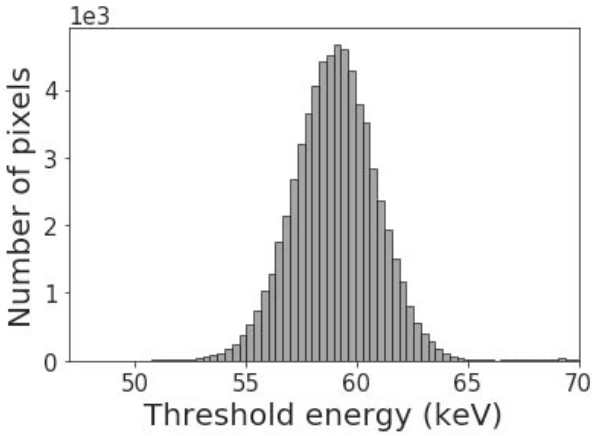

Fig. 13. Threshold dispersion measured at 58.65 keV.

The inter pixel variations can result in deviations in slopes of their individual calibration lines. Thus for any given measurement with a user specified DAC TH, the corresponding calibration energy E_p (See Eq. 14) of pixels may vary significantly from the global $\overline{E}$ (See Eq. 13), effectively reducing the detector's energy resolution. For uniform illumination across the detector and for a chosen DAC TH, this results in each pixel collecting x-rays above slightly different energies (E_p) instead of $\overline{E}$ (with a deviation $\Delta E_p = \overline{E} - E_p$), resulting in varying counts per pixel (I_p) (see Eq. 6) across the detector. Reducing the effect of gain variations and the resulting in-homogeneity in energy calibration across pixels amounts to effectively accounting for and correcting these deviations in counts. The deviation in counts (ΔI_p) for a chosen DAC TH, can be estimated as $\Delta I_p = \frac{dI_p}{dE_p}\Delta E_p$ where $\frac{dI_p}{dE_p}$ can be obtained by interpolating I_p. A map of ΔE_p across the detector pixels can be obtained following a per-pixel calibration using DIR technique as described earlier. The corrected intensity for each pixel, I_p^{corr} can now be estimated as $I_p^{corr} = I_p + \Delta I_p$; completing the corrections for per-pixel energy calibration across the detector unit.

Such pixel by pixel correction procedure following an initial global DIR based calibration method is demonstrated here with the measured K_α fluorescence line of a W target. A comparison between the measured energy spectrum before and after the per pixel spectral correction is shown in Fig. 12. For both calibration methods the figure shows the total counts (obtained by summing up photon counts of all pixels in the chip) as a function of the threshold energy, over a range of DAC thresholds corresponding to energies between 35 and 80 keV. For the per pixel calibration, the counts in each pixel were corrected as described above to account for inter-pixel variation in true energy threshold levels.

By using the global DIR calibration, a FWHM of ≈10 keV at 58.65 keV (the K_α emission line of the W) was measured, corresponding to an energy resolution of 17%. By using the pixel by pixel correction method, a FWHM of ≈7 keV, corresponding to an energy resolution of 12% was measured for the same energy. This shows how a pixel by pixel calibration significantly improves the overall PCD's energy resolution. This would be particularly useful for ASICs where interpixel gain variations are large and often much higher than what is found in Medipix detectors.

By monitoring the position of tungsten K_α emission line for each independently calibrated pixel, the DAC threshold variations between pixels can be estimated. By calculating standard deviation of the threshold energy positions among the pixels for the particular emission energy in the tungsten fluorescence, one can quantify the threshold dispersion. The measured threshold dispersion at 58.65 keV was found to be of the order of 4.48 keV, with a coefficient of threshold dispersion variation of ≈7.6% (see Fig. 13).

It is worth noting that the overall improvement in the PCD energy resolution only arises from inter pixel gain and residual threshold dispersion corrections. In principle, any robust and accurate calibration method (not necessarily the proposed DIR method) applied on a pixel to pixel basis followed by a correction in counts for each pixel to account for the variability would provide the same improvement in the overall energy resolution.

III. Conclusion

An overview of three methods used for calibrating the DAC threshold value of photon counting detectors has been presented, highlighting the strengths and the weaknesses of each method.

The XRF provides a precise method for PCD energy calibration. Its main limitation is the requirement for rearranging the experimental set up necessary for calibration. This is not always feasible in clinical imaging systems. We showed that the K-edge calibration method is limited by the detector's inherent energy resolution and by the significant detector's spectral distortion.

The conventional kVp calibration method proposed previously [26], [27] is the most practical in terms of continuously available reference energies from the x-ray tube. This method can be implemented without any additional components or targets for the calibration procedure and does not require realigning the detector as in XRF methods. However, this method does not yield robust calibration under varying flux or scan times.

In order to overcome these limitations, we propose a novel and simple alternative: a differential intensity ratios method which exploits the sharp spectral variation in the relative intensities at K-edges as well as at the kVp. The demonstrated significant insensitivity of DIR signature to detector spectral distortions and energy resolution is a key finding. The implementation of our novel approach was demonstrated for K-edge and kVp based energy calibration, offering stable and accurate results when compared to the XRF method. When applied as an alternative to conventional K-edge calibration, the DIR method allows precise localization of the K-edge transitions. This is otherwise difficult to determine because of the broadening introduced by the detector's energy resolution and spectral distortions. When used as a kVp method, the DIR offers significant stability against incident photon fluxes. The main advantage of DIR over XRF method is that no rearrangement of the source and detector positions is required. A convenient way to implement the proposed DIR method would consist of using two or more targets with K-edges simultaneously in the beam path while also exploiting the source kVp. Alternatively, one could simply apply the DIR method to multiple exposures with changing kVp values without the need for any target material in the beam path.

Finally, we demonstrated the advantages of a pixel by pixel calibration using the DIR method in improving the detector's spectral resolution. This is achieved by correcting for the count variations among pixels resulting from inter pixel gain and residual threshold dispersion variations. In this regard, the Medipix3RX is well known to feature a very good homogeneity between pixels [1]. The proposed inter pixel correction methods can be expected to yield significantly higher improvements in the overall energy resolution for detectors with more severe inter pixel variations, where a global energy calibration would be insufficient.

IV. Acknowledgements

The authors are thankful for discussions with several Medipix3 collaboration members at CERN.

References

[1] R. Ballabriga *et al.*, "The Medipix3RX: A high resolution, zero dead-time pixel detector readout chip allowing spectroscopic imaging," *J. Instrum.*, vol. 8, no. 2, p. C02016, 2013.

[2] R. Ballabriga *et al.*, "Review of hybrid pixel detector readout ASICs for spectroscopic X-ray imaging," *J. Instrum.*, vol. 11, no. 1, p. P01007, 2016.

[3] S. R. Amendolia *et al.*, "MEDIPIX: A VLSI chip for a GaAs pixel detector for digital radiology," *Nucl. Instrum. Methods Phys. Res. A, Accel. Spectrom. Detect. Assoc. Equip.*, vol. 422, nos. 1–3, pp. 201–205, 1999.

[4] J. Watt *et al.*, "Dose reductions in dental X-ray imaging using Medipix," *Nucl. Instrum. Methods Phys. Res. A, Accel. Spectrom. Detect. Assoc. Equip.*, vol. 513, nos. 1–2, pp. 65–69, 2003.

[5] L. Yu *et al.*, "Radiation dose reduction in computed tomography: Techniques and future perspective," *Imag. Med.*, vol. 1, no. 1, pp. 65–84, 2009.

[6] M. Åslund, B. Cederström, M. Lundqvist, and M. Danielsson, "Physical characterization of a scanning photon counting digital mammography system based on Si-strip detectors," *Med. Phys.*, vol. 34, no. 6, pp. 1918–1925, 2007.

[7] E. Fredenberg, M. Hemmendorff, B. Cederström, M. Åslund, and M. Danielsson, "Contrast-enhanced spectral mammography with a photon-counting detector," *Med. Phys.*, vol. 37, no. 5, pp. 2017–2029, 2010.

[8] H. Ding, H.-M. Cho, W. C. Barber, J. S. Iwanczyk, and S. Molloi, "Characterization of energy response for photon-counting detectors using X-ray fluorescence," *Med. Phys.*, vol. 41, no. 12, p. 121902, 2014.

[9] E. Roessl and R. Proksa, "K-edge imaging in X-ray computed tomography using multi-bin photon counting detectors," *Phys. Med. Biol.*, vol. 52, no. 15, p. 4679, 2007.

[10] R. E. Alvarez and A. Macovski, "Energy-selective reconstructions in X-ray computerised tomography," *Phys. Med. Biol.*, vol. 21, no. 5, p. 733, 1976.

[11] J. P. Ronaldson *et al.*, "Toward quantifying the composition of soft tissues by spectral CT with Medipix3," *Med. Phys.*, vol. 39, no. 11, pp. 6847–6857, 2012.

[12] Z. Yu *et al.*, "Evaluation of conventional imaging performance in a research whole-body CT system with a photon-counting detector array," *Phys. Med. Biol.*, vol. 61, no. 4, p. 1572, 2016.

[13] D. Gürsoy and M. Das, "Single-step absorption and phase retrieval with polychromatic X rays using a spectral detector," *Opt. Lett.*, vol. 38, no. 9, pp. 1461–1463, 2013.

[14] M. Das and Z. Liang, "Spectral X-ray phase contrast imaging for single-shot retrieval of absorption, phase, and differential-phase imagery," *Opt. Lett.*, vol. 39, no. 21, pp. 6343–6346, 2014.

[15] R. N. Wilke *et al.*, "High-flux ptychographic imaging using the new 55μm-pixel detector 'Lambda' based on the Medipix3 readout chip," *Acta Crystallographica A, Found. Adv.*, vol. 70, no. 6, pp. 552–562, 2014.

[16] K. Taguchi and J. S. Iwanczyk, "Vision 20/20: Single photon counting X-ray detectors in medical imaging," *Med. Phys.*, vol. 40, no. 10, p. 100901, 2013.

[17] T. G. Schmidt and F. Pektas, "Region-of-interest material decomposition from truncated energy-resolved CT," *Med. Phys.*, vol. 38, no. 10, pp. 5657–5666, 2011.

[18] H. Ding and S. Molloi, "Image-based spectral distortion correction for photon-counting X-ray detectors," *Med. Phys.*, vol. 39, no. 4, pp. 1864–1876, Apr. 2012.

[19] A. M. Alessio and L. R. MacDonald, "Quantitative material characterization from multi-energy photon counting CT," *Med. Phys.*, vol. 40, no. 3, p. 031108, 2013.

[20] N. R. Fredette, C. E. Lewis, and M. Das, "A multi-step method for material decomposition in spectral computed tomography," *Proc. SPIE, Phys. Imag.*, vol. 10132, 2017.
[21] T. Koenig *et al.*, "How spectroscopic X-ray imaging benefits from inter-pixel communication," *Phys. Med. Biol.*, vol. 59, no. 20, p. 6195, 2014.
[22] T. Koenig *et al.*, "Charge summing in spectroscopic X-ray detectors with high-Z sensors," *IEEE Trans. Nucl. Sci.*, vol. 60, no. 6, pp. 4713–4718, Dec. 2013.
[23] R. Ballabriga, M. Campbell, E. Heijne, X. Llopart, L. Tlustos, and W. Wong, "Medipix3: A 64 k pixel detector readout chip working in single photon counting mode with improved spectrometric performance," *Nucl. Instrum. Methods Phys. Res. A, Accel. Spectrom. Detect. Assoc. Equip.*, vol. 633, pp. S15–S18, May 2011.
[24] E. N. Gimenez *et al.*, "Characterization of Medipix3 with synchrotron radiation," *IEEE Trans. Nucl. Sci.*, vol. 58, no. 1, pp. 323–332, Feb. 2011.
[25] H.-M. Cho, H. Ding, B. P. Ziemer, and S. Molloi, "Energy response calibration of photon-counting detectors using X-ray fluorescence: A feasibility study," *Phys. Med. Biol.*, vol. 59, no. 23, p. 7211, 2014.
[26] R. K. Panta, M. F. Walsh, S. T. Bell, N. G. Anderson, A. P. Butler, and P. H. Butler, "Energy calibration of the pixels of spectral X-ray detectors," *IEEE Trans. Med. Imag.*, vol. 34, no. 3, pp. 697–706, Mar. 2015.
[27] M. Das, B. Kandel, C. S. Park, and Z. Liang, "Energy calibration of photon counting detectors using X-ray tube potential as a reference for material decomposition applications," *Proc. SPIE, Phys. Imag.*, vol. 9412, 2015.
[28] K. Taguchi, E. C. Frey, X. Wang, J. S. Iwanczyk, and W. C. Barber, "An analytical model of the effects of pulse pileup on the energy spectrum recorded by energy resolved photon counting X-ray detectors," *Med. Phys.*, vol. 37, no. 8, pp. 3957–3969, Aug. 2010.
[29] E. Frojdh *et al.*, "Count rate linearity and spectral response of the Medipix3RX chip coupled to a 300μm silicon sensor under high flux conditions," *J. Instrum.*, vol. 9, no. 4, p. C04028, 2014.
[30] *NIST XCOM Data*. Accessed: Mar. 20, 2017. [Online]. Available: https://physics.nist.gov/PhysRefData/Xcom/html/xcom1.html
[31] Y. Ge, X. Ji, R. Zhang, K. Li, and G.-H. Chen, "K-edge energy-based calibration method for photon counting detectors," *Phys. Med. Biol.*, vol. 63, no. 1, p. 015022, 2017.
[32] J. S. Lee, D.-G. Kang, S. O. Jin, I. Kim, and S. Y. Lee, "Energy calibration of a CdTe photon counting spectral detector with consideration of its non-convergent behavior," *Sensors*, vol. 16, no. 4, p. 518, 2016.
[33] R. W. Schafer, "What is a savitzky-golay filter? [lecture notes]," *IEEE Signal Process. Mag.*, vol. 28, no. 4, pp. 111–117, Jul. 2011.